Article

Anion Template Effect on the Self-Assembly and Interconversion of Metallacyclophanes

Cristian Saul Campos-Fernndez, Brandi L. Schottel, Helen T. Chifotides, Jitendra K. Bera, John Bacsa, John M. Koomen, David H. Russell, and Kim R. Dunbar

J. Am. Chem. Soc., **2005**, 127 (37), 12909-12923• DOI: 10.1021/ja052108q • Publication Date (Web): 27 August 2005

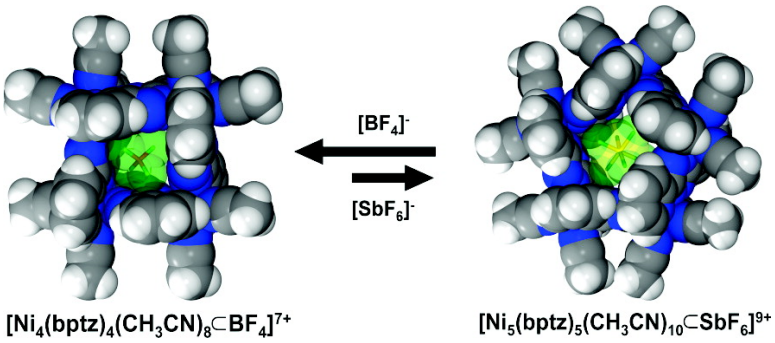

More About This Article

Additional resources and features associated with this article are available within the HTML version:

- Supporting Information
- Links to the 30 articles that cite this article, as of the time of this article download
- Access to high resolution figures
- Links to articles and content related to this article
- Copyright permission to reproduce figures and/or text from this article

View the Full Text HTML

J|A|C|S
ARTICLES
Published on Web 08/27/2005

Anion Template Effect on the Self-Assembly and Interconversion of Metallacyclophanes

Cristian Saul Campos-Fernández, Brandi L. Schottel, Helen T. Chifotides, Jitendra K. Bera, John Bacsa, John M. Koomen, David H. Russell, and Kim R. Dunbar*

Contribution from the Department of Chemistry, Texas A&M University, College Station, Texas 77842

Received April 2, 2005; E-mail: dunbar@mail.chem.tamu.edu

Abstract: Reactions of 3,6-bis(2-pyridyl)-1,2,4,5-tetrazine (bptz) with solvated first-row transition metals M(II) (M(II) = Ni, Zn, Mn, Fe, Cu) have been explored with emphasis on the factors that influence the identity of the resulting cyclic products for Ni(II) and Zn(II). The relatively small anions, namely $[ClO_4]^-$ and $[BF_4]^-$, lead to the formation of molecular squares $[\{M_4(bptz)_4(CH_3CN)_8\}\subset X][X]_7$, (M = Zn(II), Ni(II); X = $[BF_4]^-$, $[ClO_4]^-$), whereas the larger anion $[SbF_6]^-$ favors the molecular pentagon $[\{Ni_5(bptz)_5(CH_3CN)_{10}\}\subset SbF_6][SbF_6]_9$. The molecular pentagon easily converts to the square in the presence of excess $[BF_4]^-$, $[ClO_4]^-$, and $[I]^-$ anions, whereas the Ni(II) square can be partially converted to the less stable pentagon under more forcing conditions in the presence of excess $[SbF_6]^-$ ions. No evidence for the molecular square being in equilibrium with the pentagon was observed in the ESI-MS spectra of the individual square and pentagon samples. Anion-exchange reactions of the encapsulated ion in $[\{Ni_4(bptz)_4(CH_3CN)_8\}\subset ClO_4][ClO_4]_7$ reveal that a larger anion such as $[IO_4]^-$ cannot replace $[ClO_4]^-$ inside the cavity, but that the linear $[Br_3]^-$ anion is capable of doing so. ESI-MS studies of the reaction between $[Ni(CH_3CN)_6][NO_3]_2$ and bptz indicate that the product is trinuclear. Mass spectral studies of the bptz reactions with Mn(II), Fe(II), and Cu(II), in the presence of $[ClO_4]^-$ anions, support the presence of molecular squares. The formation of the various metallacyclophanes is discussed in light of the factors that influence these self-assembly reactions, such as choice of metal ion, anion, and solvent.

Introduction

Traditional synthetic chemistry involves the design of molecules by the stepwise formation of covalent bonds in a prearranged fashion. Such an approach is not feasible, however, for the high-yield syntheses of large, complex molecules from multiple building blocks. Instead, one must turn to self-assembly reactions that rely on the connection of individual building blocks via noncovalent interactions. To achieve the formation of a single product in high yield, the precursors of the self-assembled structures must be stable and relatively rigid, whereas the bonds that join the components should be sufficiently labile such that the formation of the supramolecular assembly is ultimately under thermodynamic control. The final product represents a minimum in the energy profile of the system based on a combination of enthalpic and entropic factors.[1]

Transition metal coordination bonds satisfy the aforementioned criteria and have been exploited for the synthesis of numerous metal-based supramolecular architectures in recent years.[2] Metal ion complexation by multidentate ligands generates equilibrium mixtures of cyclic and open-frame oligomeric structures depending on the number and geometry of the individual building blocks. The factors that influence the size and shape of these structures are complex and include the

(1) (a) Leininger, S.; Olenyuk, B.; Stang, P. J. *Chem. Rev.* **2000**, *100*, 853. (b) Lehn, J.-M. *Supramolecular Chemistry: Concepts and Perspectives*; VCH: Weinheim, 1995. (c) Steed, J. W.; Atwood, J. L. *Supramolecular Chemistry*; John Wiley: New York, 2001. (d) Davis, A. V.; Yeh, R. M.; Raymond, K. N. *Proc. Natl. Acad. Sci. U.S.A.* **2002**, *99*, 4793.

(2) (a) Davis, A. V.; Raymond, K. N. *J. Am. Chem. Soc.* **2005**, *127*, 7912. (b) Mukherjee, P. S.; Min, K. S.; Arif, A. M.; Stang, P. J. *Inorg. Chem.* **2004**, *43*, 6345. (c) Atwood, J. L.; Barbour, L. J.; Dalgarno, S. J.; Hardie, M. J.; Raston, C. L.; Webb, H. R. *J. Am. Chem. Soc.* **2004**, *126*, 13170. (d) Uppadine, L. H.; Lehn, J.-M. *Angew. Chem., Int. Ed.* **2004**, *43*, 240. (e) Ruben, M.; Rojo, J.; Romero-Salguero, F. J.; Uppadine, L. H.; Lehn, J.-M. *Angew. Chem., Int. Ed.* **2004**, *43*, 3644. (f) Sun, S.-S.; Stern, C. L.; Nguyen, S.-B. T.; Hupp, J. T. *J. Am. Chem. Soc.* **2004**, *126*, 6314. (g) Kryschenko. Y. K.; Seidel, S. R.; Muddiman, D. C.; Nepomuceno, A. I.; Stang, P. J. *J. Am. Chem. Soc.* **2003**, *125*, 9647. (h) Kryschenko, Y. K.; Seidel, S. R.; Arif, A. M.; Stang, P. J. *J. Am. Chem. Soc.* **2003**, *125*, 5193. (i) Patroniak, V.; Baxter, P. N. W.; Lehn, J.-M.; Kubicki, M.; Nissinen, M.; Rissanen, K. *Eur. J. Inorg. Chem.* **2003**, 4001. (j) Goshe, A. J.; Steele, I. M.; Ceccarelli, C.; Rheingold, A. L.; Bosnich, B. *Proc. Natl. Acad. Sci. U.S.A.* **2002**, *99*, 4823. (k) Oxtoby, N. S.; Blake, A. J.; Champness, N. R.; Wilson, C. *Proc. Natl. Acad. Sci. U.S.A.* **2002**, *99* 4905. (l) Kuehl, C. J.; Kryshenko, Y. K.; Radhakrishnan, U.; Seidel, S. R.; Huang, S. D.; Stang, P. J. *Proc. Natl. Acad. Sci. U.S.A.* **2002**, *99*, 4932. (m) Holliday, B. J.; Mirkin, C. A. *Angew. Chem., Int. Ed.* **2001**, *40*, 2022. (n) Eddaoudi, M.; Moler, D. B.; Li, H.; Chen, B.; Reineke, T. M.; O'Keeffe, M.; Yaghi, O. M. *Acc. Chem. Res.* **2001**, *34*, 319. (o) Cotton, F. A.; Lin, C.; Murillo, C. A. *Acc. Chem. Res.* **2001**, *34*, 759. (p) Bera, J. K.; Smucker, B. W.; Walton, R. A.; Dunbar, K. R. *Chem. Commun.* **2001**, 2562. (q) Greig, L. M.; Philip, D. *Chem. Soc. Rev.* **2001**, *30*, 287. (r) Johnson, D. W.; Raymond, K. N. *Supramol. Chem.* **2001**, *13*, 639. (s) Nguyen, S.-B. T.; Gin, D. L.; Hupp, J. T.; Zhang, X. *Proc. Natl. Acad. Sci. U.S.A.* **2001**, *98*, 11849. (t) Swiegers, G. F.; Malefetse, T. J. *Chem. Rev.* **2000**, *100*, 3483. (u) Sun, S.-S.; Lees, A. J. *J. Am. Chem. Soc.* **2000**, *122*, 8956. (v) Caulder, D. L.; Raymond, K. N. *Acc. Chem. Res.* **1999**, *32*, 975. (w) Navarro, J. A. R.; Lippert, B. *Coord. Chem. Rev.* **1999**, *185*−*186*, 653. (x) Schnebeck, R.-D.; Freisinger, E.; Lippert, B. *Angew. Chem., Int. Ed.* **1999**, *38*, 168. (y) Fujita, M. *Acc. Chem. Res.* **1999**, *32*, 53.

number, relative strength, and directionality of weak interactions between the building blocks.[3] The product distribution of a particular reaction under thermodynamic control is dictated by the relative free energies of the products,[4] whereas the stability of a given cyclic product is determined, to some extent, by the ring strain of the molecule as well as by the concentration of the starting materials.[5] Dilute solutions favor ring closure, whereas concentrated solutions result in the isolation of infinite polymers. Self-assembly reactions may also depend on a variety of other parameters, such as temperature, pressure, and identity of the solvent.

Armed with increasing knowledge of noncovalent interactions,[6] chemists have applied the tools of molecular recognition to favor a desired supramolecular entity. A useful approach in this vein is the use of a chemical species that selectively recognizes and stabilizes the desired product in a mixture via supramolecular interactions. This species is commonly referred to as a template, and it may be considered as the controlling element in the synthetic pathway of a thermodynamically or kinetically controlled self-assembly process.[7] The template can be a permanent part of the final product or simply a temporary helper that is not required to maintain the integrity of the final product.

The role of anions in self-assembly processes has emerged as an increasingly active theme in the recent literature.[8] Anions chosen for their "relative innocence" in terms of coordinating ability can nevertheless direct the course of an assembly process via noncovalent interactions. The capacity of anions to act as templates was not fully appreciated until recently, despite the fact that the first example of an encapsulated anion system was reported during the nascence of supramolecular chemistry.[9] Clearly, this work on katapinates reported by Park et al.[9] was somewhat obscured by Pedersen's discovery of cation-encapsulating crown ethers.[10] Since the work of Hawthorne et al., beginning a decade ago,[11] however, reports on the role of anions in the self-assembly of transition metal systems have increased, although there are still far fewer examples in comparison to analogous studies involving cations. One of the reasons for the relative dearth of reports devoted to anions is the greater challenge to design molecules templated by anions as compared to cation-assisted processes.[12] Anions are typically larger than cations, they are electronically "saturated" and display a wide range of coordination geometries, are often pH sensitive, and exhibit much higher free energies of solvation.[8h]

Chart 1

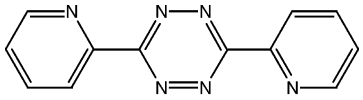

bptz

Herein, we report a comprehensive investigation of an anion-templated self-assembly reaction, namely that of solvated first-row transition metal ions M(II) (M = Ni, Zn, Mn, Fe, Cu) with the divergent bis-bipyridine ligand 3,6-bis(2-pyridyl)-1,2,4,5-tetrazine (bptz; Chart 1). The molecular polygons $[\{Ni_4(bptz)_4(CH_3CN)_8\}\subset BF_4][BF_4]_7$[13a] and $[\{Ni_5(bptz)_5(CH_3CN)_{10}\}\subset SbF_6][SbF_6]_9$,[13b] in the presence of the appropriate anions, have been reported in preliminary communication form. The combined results of X-ray crystallography, mass spectrometry, and NMR studies provide compelling evidence that the anions play a decisive role in the formation of a particular cyclic structure both in the solid state and in solution.

Experimental Section

Materials. All manipulations were carried out under an inert atmosphere of N_2 gas with the use of drybox and Schlenk-line techniques. Acetonitrile, methanol, dichloromethane, tetrahydrofuran (THF), benzene, and toluene were dried by conventional methods, distilled over nitrogen, and deoxygenated prior to use. The compounds $[Ni(CH_3CN)_6][X]_2$ (X = $[BF_4]^-$, $[SbF_6]^-$, or $[CF_3SO_3]^-$), $[Zn(CH_3CN)_4][BF_4]_2$, and $[Mn(CH_3CN)_6][BF_4]_2$ were synthesized by literature procedures.[14] The salts $M(ClO_4)_2 \cdot xH_2O$ (M = Ni(II), Zn(II), Mn(II), Fe(II), Cu(II)) were purchased from Aldrich and used without further purification. (**Caution!** *Perchlorate salts of metal complexes with organic ligands are potential explosives. While we have encountered no incidents in the preparation and reactivity studies of the salts, it is advisable to use only small amounts and to handle the compounds with caution in the presence of wet solvents.*) The bptz ligand was prepared by a literature method and recrystallized from benzene.[15] The tetra-*n*-butylammonium salts of iodide, nitrate, periodate, tetrafluoroborate, hexafluorophosphate, and tribromide were purchased from Aldrich and used without further purification.

Physical Measurements. Infrared spectra were recorded in the range 4000−400 cm^{-1} using a Nicolet 470 FT-IR spectrometer on Nujol mull samples suspended between KBr plates. The ^1H NMR spectra were recorded on a 500 MHz Inova spectrometer with a 5-mm switchable probehead. The ^{19}F and ^{11}B NMR spectra were recorded on a 400 MHz Unity Inova spectrometer with a 5-mm autoswitchable probe operating at 375.99 and 128.22 MHz, respectively. The ^1H NMR spectra were referenced relative to the residual proton impurities of the deuterated solvent (CD_3CN-d_3). The ^{19}F NMR spectra were referenced relative to $CFCl_3$ (0 ppm), whereas the ^{11}B NMR spectra were referenced relative to BF_3 in $CHCl_3$ at 0 ppm. Electrospray mass spectra were obtained with a Sciex Qstar Pulsar and a Protana Nanospray ion source. Data were acquired with a TOFMA 2.0RC3 and analyzed with BioMultiView 1.5RC3. Solutions of the metal complexes were diluted to approximately 10 μM, and 7.0 μL aliquots were loaded into the Au/Pd-coated silica spray needle. Ion spray voltages were set between 900 and 1200 V.

(3) Olenyuk, B.; Fechtenkötter, A.; Stang, P. J. *J. Chem. Soc., Dalton Trans.* **1998**, 1707.
(4) Claderone, C. T.; Williams, D. H. *J. Am. Chem. Soc.* **2001**, *123*, 6262.
(5) (a) Kuehl, C. J.; Huang, S. D.; Stang, P. J. *J. Am. Chem. Soc.* **2001**, *123*, 9634. (b) Yamamoto, T.; Arif, A. M.; Stang, P. J. *J. Am. Chem. Soc.* **2003**, *125*, 12309.
(6) Müller-Dethlefs, K.; Hobza, P. *Chem. Rev.* **2000**, *100*, 143.
(7) Furlan, R. L. E.; Otto, S.; Sanders, J. K. M. *Proc. Natl. Acad. Sci. U.S.A.* **2002**, *99*, 4801.
(8) (a) Kim, H.-J.; Zin, W.-C.; Lee, M. *J. Am. Chem. Soc.* **2004**, *126*, 7009. (b) Coles, S. J.; Frey, J. G.; Gale, P. A.; Hursthouse, M. B.; Light, M. E.; Navakhun, K.; Thomas, G. L. *Chem. Commun.* **2003**, 1462. (c) Gale, P. A. *Coord. Chem. Rev.* **2003**, *240*, 191. (d) Vilar, R. *Angew. Chem., Int. Ed.* **2003**, *42*, 1460. (e) Atwood, J. L.; Szumna, A. *Chem. Commun.* **2003**, 940. (f) Schweiger, M.; Seidel, S. R.; Arif, A. M.; Stang, P. J. *Inorg. Chem.* **2002**, *41*, 2556. (g) Gale, P. A. *Coord. Chem. Rev.* **2001**, *213*, 79. (h) Cheng, S.-T.; Doxiadi, E.; Vilar, R.; White, A. J. P.; Williams, D. J. *J. Chem. Soc., Dalton Trans.* **2001**, 2239. (i) Beer, P. D.; Gale, P. A. *Angew. Chem., Int. Ed.* **2001**, *40*, 486 and references therein. (j) Gale, P. A. *Coord. Chem. Rev.* **2000**, *199*, 181. (k) Vilar, R.; Mingos, D. M. P.; White, A. J. P.; Williams, D. J. *Angew. Chem., Int. Ed.* **1998**, *37*, 1258. (l) Beer, P. D. *Acc. Chem. Res.* **1998**, *31*, 71.
(9) Park, C. H.; Simmons, H. E. *J. Am. Chem. Soc.* **1968**, *90*, 2431.
(10) Pedersen, C. J. *J. Am. Chem. Soc.* **1967**, *89*, 7017.
(11) (a) Yang, X.; Knobler, C. B.; Zheng, Z.; Hawthorne, M. F. *J. Am. Chem. Soc.* **1994**, *116*, 7142. (b) Hawthorne, M. F.; Yang, X.; Zheng, Z. *Pure Appl. Chem.* **1994**, *66*, 245.
(12) Atwood, J. L. Structural and Topological Aspects of Anion Coordination. In *Supramolecular Chemistry of Anions*; Bianchi, A., Bowman-James, K., García-España, E., Eds.; John Wiley-VCH: New York, 1997; p 147.
(13) (a) Campos-Fernández, C. S.; Clérac, R.; Dunbar, K. R. *Angew. Chem., Int. Ed.* **1999**, *38*, 3477. (b) Campos-Fernández, C. S.; Clérac, R.; Koomen, J. M.; Russell, D. H.; Dunbar, K. R. *J. Am. Chem. Soc.* **2001**, *123*, 773.
(14) Heintz, R. A.; Smith, J. A.; Szalay, P. S.; Weisgerber, A.; Dunbar, K. R. *Inorg. Synth.* **2002**, *33*, 75.
(15) Geldard, J. F.; Lions, F. *J. Org. Chem.* **1965**, *30*, 318.

Theoretical isotope ratio calculations were performed using the program ISOPRO3.0.[16]

Syntheses. Preparation of $[Ni_4(bptz)_4(CH_3CN)_8][BF_4]_8$ (1). A fuchsia solution (10 mL) of bptz (50 mg, 0.21 mmol) in CH_3CN was added slowly to a blue solution of $[Ni(CH_3CN)_6][BF_4]_2$ (100 mg, 0.21 mmol) in CH_3CN (10 mL). As the mixture was stirred for 8 h, it turned from dark green to brown-green. The resulting solution was concentrated and layered over 10 mL of toluene. After 7 days, the brown-green microcrystalline solid that had formed was collected by filtration, washed with benzene (3 × 5 mL), and dried in vacuo. Yield: 97 mg (84%). Anal. Calcd for $Ni_4C_{64}N_{32}H_{56}B_8F_{32}$: C, 34.90; N, 20.35; H, 2.56. Found: C, 35.21; N, 19.83; H, 2.52. IR (KBr mull, cm^{-1}): 2321, 2325 (w, ν(C≡N)), 1064 (s, ν(B−F)). UV−vis (λ, nm (ϵ, M^{-1} cm^{-1})): 510 (530), 680 (266). ES-MS: *m*/*z* 1787.3 $[Ni_4(bptz)_4(BF_4)_7]^+$.

Preparation of $[Ni_4(bptz)_4(CH_3CN)_8][ClO_4]_8$ (2). A procedure similar to that described for the synthesis of **1** was carried out with $Ni(ClO_4)_2 \cdot 6H_2O$ (106 mg, 0.29 mmol) and bptz (50 mg, 0.21 mmol). One hour after addition of the two reagents, the solution changed from dark green to brown-green. The solution was stirred overnight and layered over THF. The dark brown microcrystals of **2** that formed were separated from the solution by filtration. Yield: 111 mg (92%). Anal. Calcd for $Ni_4C_{64}N_{32}H_{56}Cl_8O_{32}$: C, 33.37; N, 19.46; H, 2.45. Found: C, 33.34; N, 18.93; H, 2.48. IR (KBr mull, cm^{-1}): 2321, 2325 (w, sh, ν(C≡N)), 1098 (s, br, ν(Cl−O)). UV−vis (λ, nm (ϵ, M^{-1} cm^{-1})): 510 (530), 680 (266). ES-MS: *m*/*z* 1875.8 $[Ni_4(bptz)_4(ClO_4)_7]^+$.

Preparation of $[Zn_4(bptz)_4(CH_3CN)_8][BF_4]_8$ (3). A fuchsia solution of bptz (50 mg, 0.21 mmol) in CH_3CN (10 mL) was added dropwise to a colorless solution of $[Zn(CH_3CN)_4][BF_4]_2$ (85 mg, 0.21 mmol) in CH_3CN. Upon addition, an obvious change of the solution from colorless to orange was observed. The reaction solution was stirred for 12 h, concentrated, and layered over 10 mL of benzene. After several days, an orange solid was collected by filtration, washed with CH_2Cl_2 (3 × 5 mL), and dried in vacuo. Yield: 84 mg (72%). Anal. Calcd for $Zn_4C_{64}N_{32}H_{56}B_8F_{32}$: C, 34.48; N, 20.11; H, 2.53. Found: C, 34.11; N, 19.69; H, 2.48. IR (KBr mull, cm^{-1}): 1054 (s, ν(B−F)). UV−vis (λ, nm (ϵ, M^{-1} cm^{-1})): 540 (270). ES-MS: *m*/*z* 1814.1 $[Zn_4(bptz)_4(BF_4)_7]^+$. ^1H NMR (CD_3CN-d_3, δ, ppm): 8.10 (d, 8H, 3,3′-H), 8.31 (ddd, 8H, 5,5′-H), 8.52 (ddd, 8H, 4,4′-H), 9.25 (dd, 8H, 6,6′-H), 2.49 (s, CH_3-CN-d_3). ^{19}F NMR (CD_3CN-d_3, 22 °C, δ, ppm): −151 ($[BF_4]^-$ free ions). ^{19}F NMR (CD_3CN-d_3, −15 °C, δ, ppm): −151 ($[BF_4]^-$ free ions), −144 ($[BF_4]^-$ encapsulated ions). ^{11}B NMR (CD_3CN-d_3, δ, ppm): 3.6 ($[BF_4]^-$).

Preparation of $[Zn_4(bptz)_4(CH_3CN)_8][ClO_4]_8$ (4). A procedure similar to that described for the synthesis of **3** was carried out using $Zn(ClO_4)_2 \cdot 6H_2O$ (90 mg, 0.24 mmol) and bptz (50 mg, 0.21 mmol). Yield: 105 mg (86%). Anal. Calcd for $Zn_4C_{64}N_{32}H_{56}Cl_8O_{32}$: C, 32.98; N, 19.23; H, 2.42. Found: C, 33.13; N, 18.74; H, 2.43. IR (KBr mull, cm^{-1}): 1098 (s, br, ν(Cl−O)). UV−vis (λ, nm (ϵ, M^{-1} cm^{-1})): 540 (270). ES-MS: *m*/*z* 1902.6 $[Zn_4(bptz)_4(ClO_4)_7]^+$. ^1H NMR (CD_3CN-d_3, δ, ppm): 8.13 (d, 8H, 3,3′-H), 8.32 (ddd, 8H, 5,5′-H), 8.50 (ddd, 8H, 4,4′-H), 9.24 (dd, 8H, 6,6′-H), 2.50 (s, CH_3CN).

Preparation of $[Ni_5(bptz)_5(CH_3CN)_{10}][SbF_6]_{10}$ (5). A procedure similar to that described for the synthesis of **1** was carried out using $[Ni(CH_3CN)_6][SbF_6]_2$ (163 mg, 0.21 mmol) and bptz (50 mg, 0.21 mmol). Analytically pure material was obtained by layering an acetonitrile solution of the compound over toluene. Yield: 160 mg (90%). Anal. Calcd for $Ni_5C_{80}H_{70}N_{40}Sb_{10}F_{60}$: C, 22.65; N, 13.21; H, 1.66. Found: C, 22.70; N, 12.81; H, 1.61. IR (KBr mull, cm^{-1}): 2320, 2318 (w, ν(C≡N)). UV−vis (λ, nm (ϵ, M^{-1} cm^{-1})): 510 (540), 690 (260). ES-MS: *m*/*z* 3596.3 $[Ni_5(bptz)_5(SbF_6)_9]^+$.

Preparation of $[Ni_3(bptz)_3][NO_3]_6$ (6). A solution of $[n\text{-}Bu_4N][NO_3]$ (32 mg, 0.10 mmol) in acetonitrile (10 mL) was added to 42.4 mg of **5** (0.01 mmol) dissolved in 10 mL of acetonitrile. An instantaneous precipitation of a yellow solid was observed. The reaction mixture was stirred for an additional 2 h. The solid was collected by filtration, washed with CH_3CN (3 × 5 mL) followed by CH_2Cl_2 (3 × 5 mL), and dried in vacuo. Yield: 19.5 mg (93%). Anal. Calcd for $Ni_3C_{36}N_{24}H_{24}O_{18}$: C, 34.40; N, 26.75; H, 1.93. Found: C, 34.36; N, 26.33; H, 1.91. IR (KBr mull, cm^{-1}): 1475 (ν(N═O)), 1293 ($\nu(NO_2)$). ES-MS: *m*/*z* 1194.7 $[Ni_3(bptz)_3(NO_3)_5]^+$.

An alternative synthetic route consists of treating a bptz solution (10 mL) of bptz (50 mg, 0.21 mmol) with $[Ni(CH_3CN)_6][NO_3]_2$ (90 mg, 0.21 mmol) in acetonitrile (10 mL). After 2 h, a yellow-brown solid was collected by filtration, washed with benzene (3 × 5 mL), and dried in vacuo. Yield: 60 mg (68%).

Preparation of $[Ni_4(bptz)_4(CH_3CN)_8][SbF_6]_7[I]$ (7). An acetonitrile solution (10 mL) of $[n\text{-}Bu_4N][I]$ (7.4 mg, 0.02 mmol) was added to a stirring solution of **5** (42.4 mg, 0.01 mmol) in CH_3CN, and the mixture was stirred for 2 h. The resulting brown solution was filtered, concentrated, and layered over benzene (20 mL). The brown solid that appeared after several days was collected by filtration, washed with benzene (3 × 5 mL), and dried in vacuo. Yield: 30 g (73%). Anal. Calcd for $Ni_4C_{64}N_{32}H_{56}Sb_7F_{42}I$: C, 23.40; N, 13.64; H, 1.72. Found: C, 23.63; N, 13.68; H, 1.81.

Preparation of $[Ni_4(bptz)_4(CH_3CN)_8][BF_4][PF_6][SbF_6]_6$ (8). An acetonitrile solution (10 mL) of **5** (25.4 mg, 0.006 mmol) was layered over an equimolar mixture of $[n\text{-}Bu_4N][BF_4]$ (8.9 mg, 0.027 mmol) and $[n\text{-}Bu_4N][PF_6]$ (10.1 mg, 0.026 mmol) in CH_2Cl_2. The yellow-brown solid that appeared after several days was collected by filtration, washed with benzene (3 × 5 mL), and dried in vacuo. Yield: 9 mg (46%).

Preparation of $[Ni_4(bptz)_4(CH_3CN)_4(H_2O)_4][ClO_4][IO_4]_7$ (9). A procedure similar to that described for the synthesis of **8** was carried out with **2** (23 mg, 0.01 mmol) dissolved in acetonitrile and a methanol solution of $[n\text{-}Bu_4N][IO_4]$ (69.2 mg, 0.16 mmol). The crop of brown crystals that grew at the interface of the two solvents was filtered, washed with benzene (3 × 5 mL), and dried in vacuo. Yield: 16 mg (56%).

Preparation of $[Ni_4(bptz)_4Br_7(CH_3CN)Br_3]$ (10). An acetonitrile solution (10 mL) of **2** (23 mg, 0.01 mmol) was diffused into a 1:2 dichloromethane/toluene solution of $[n\text{-}Bu_4N][Br_3]$ (29 mg, 0.06 mmol). Crystals grew at the interface of the two solvents over two weeks and were filtered, washed with CH_2Cl_2 (3 × 5 mL), and dried in vacuo. Yield: 15 mg (74%). Anal. Calcd for $Ni_4C_{50}N_{25}H_{35}Br_{10}$: C, 29.73; N, 17.34; H, 1.75. Found: C, 29.69; N, 16.91; H, 1.80.

Preparation of $[Ni_2(bptz)(CH_3CN)_8][ClO_4]_4$ (11). A crop of single crystals was obtained by layering diethyl ether on the filtrate obtained after harvesting the bulk sample of **2**. The approximate yield of crystals was less than 5%.

Preparation of $\{[Mn(bptz)(CH_3CN)_2][BF_4]_2\}_\infty$ (12). An acetonitrile solution (10 mL) of $[Mn(CH_3CN)_6][BF_4]_2$ (52.2 mg, 0.11 mmol) was layered over a dichloromethane solution (10 mL) of bptz (26 mg, 0.11 mmol) in a Schlenk tube. After one month, light-orange crystals of **12** intimately mixed with an unidentified green amorphous solid were obtained. Yield: 18 mg (30%).

X-ray Crystallographic Studies. Single crystal X-ray data were collected on a Bruker SMART CCD-based X-ray diffractometer with 1.5 kW graphite-monochromated Mo Kα radiation (λ = 0.71073 Å) at T = 110(2) K. Data reduction, cell refinements, and corrections for Lorentz and polarization effects were carried out with the SAINT program.[17] An empirical absorption correction was carried out by using the SADABS program.[18] The structures were solved and refined using X-SEED,[19] a graphical interface to SHELX.[20] Additional crystal-

(16) Senko, M. *ISOPRO 3.0*; Sunnyvale, CA (http://members.aol.com/msmssoft).

(17) *SAINT, Program for area detector absorption correction*; Siemens Analytical X-Ray Instruments Inc.: Madison, WI, 1994−1996.

(18) Sheldrick, G. M. *SADABS, Program for Siemens area detector absorption correction*; University of Göttingen: Göttingen, Germany, 1996.

(19) (a) Barbour, L. J. *X-Seed, Graphical interface to SHELX-97 and POV-Ray*; 1999 (http://www.x-seed.net). (b) Barbour, L. J. *J. Supramol. Chem.* **2001**, *1*, 189. (c) Atwood, J. L.; Barbour, L. J. *Cryst. Growth Des.* **2003**, *3*, 3.

lographic calculations were performed with the PLATON[21] and PARST[22] programs. In many cases the diffraction intensities were weak (even after prolonged exposures), which is attributed to disorder and loss of interstitial solvent molecules. Disordered solvent molecules with fractional site occupancies were observed in several of the structures. A summary of experimental details and pertinent crystallographic data for complexes **1**−**3**, **5**, and **7**−**12** is provided in Table 1. Selected bond distances and angles are provided in the corresponding figure caption of each structure.

[{Ni$_4$(bptz)$_4$(CH$_3$CN)$_8$}⊂BF$_4$][BF$_4$]$_7$·4CH$_3$CN (1·4CH$_3$CN). Dark green single crystals were grown by diffusion of toluene into a solution of compound **1** in acetonitrile. Compound **1** crystallizes in the triclinic system, space group $P\bar{1}$. Five of the eight $[BF_4]^-$ ions were found to be disordered and were modeled in two orientations with restraints on the B−F and F···F distances. The $[BF_4]^-$ anion inside the cavity of the square is disordered, with the two major components being situated in a direction perpendicular to the plane of the square. The site occupancies were determined to be 0.757(8) and 0.243(8).

[{Ni$_4$(bptz)$_4$(CH$_3$CN)$_8$}⊂ClO$_4$][ClO$_4$]$_7$·4CH$_3$CN·C$_4$H$_8$O (2·4CH$_3$CN·C$_4$H$_8$O). Dark brown platelet crystals were grown by layering an acetonitrile solution of compound **2** over THF. Compound **2** crystallizes in the monoclinic system, space group $P2_1/n$. Partially occupied THF and acetonitrile molecules were refined with individual site occupancies equal to 0.5. All non-hydrogen atoms belonging to non-disordered groups were refined anisotropically. Two of the seven perchlorate ions located outside the square were disordered and modeled appropriately. The $[ClO_4]^-$ anion residing in the cavity of the square revealed no signs of disorder.

[{Zn$_4$(bptz)$_4$(CH$_3$CN)$_8$}⊂BF$_4$][BF$_4$]$_7$·4CH$_3$CN (3·4CH$_3$CN). Crystals were grown by slow diffusion of benzene into an acetonitrile solution of **3**. Compound **3** crystallizes in the triclinic system, space group $P\bar{1}$. The $[BF_4]^-$ anion residing in the cavity of the square is disordered over two positions. Geometric restraints were applied to one of the bptz ligands and to the disordered $[BF_4]^-$ anions. In the final stages of refinement, all non-hydrogen atoms were refined anisotropically.

[{Ni$_5$(bptz)$_5$(CH$_3$CN)$_{10}$}⊂SbF$_6$][SbF$_6$]$_9$·2CH$_3$CN (5·2CH$_3$CN). Crystals were grown by layering an acetonitrile solution of compound **5** over toluene. Compound **5** crystallizes in the monoclinic system, space group $C2/c$. All the $[SbF_6^-]$ ions are severely disordered, which accounts for the higher than usual R factors. The encapsulated $[SbF_6]^-$ is also disordered, with two closely spaced (Sb···Sb = 0.744(2)Å) components in different orientations.

[{Ni$_4$(bptz)$_4$(CH$_3$CN)$_8$}⊂I][SbF$_6$]$_7$ (7). Crystals were grown by diffusion of an acetonitrile solution of **7** into toluene (20 mL). Indexing of the diffraction patterns gave an approximate cell and established that the crystals belong to the orthorhombic system and one of the following space groups: $I222$, $Imm2$, $Immm$, or $I2_12_12_1$. These space groups were tested, and the structure was ultimately solved and refined in the chiral space group $I222$, despite the fact that the absolute structure parameter is 0.5(1).[23] The low standard deviation for this parameter indicated that twinning rather than a noncentrosymmetric structure was responsible for the Flack parameter. No additional crystallographic symmetry was detected from the atomic coordinates, thereby confirming merohedral twinning by inversion. The inversion twin law is −1 0 0, 0 −1 0, 0 0 −1, and the twin populations refined to 50(5):50(5) (with a Flack parameter of 0). The cation $[\{Ni_4(bptz)_4(CH_3CN)_8\}\subset I]^{7+}$ resides on a 222 symmetery element with the iodide ion positioned at the center of $[Ni_4(bptz)_4(CH_3CN)_8]^{8+}$. The $[SbF]_6^-$ ion, located on a general position, is slightly disordered. In the final cycles of refinement, all non-hydrogen and non-disordered atoms were refined anisotropically.

[{Ni$_4$(bptz)$_4$(CH$_3$CN)$_8$}⊂BF$_4$][PF$_6$][SbF$_6$]$_6$ (8). Crystals were obtained by layering an acetonitrile solution of **8** with toluene. The crystals belong to the orthorhombic system, space group $I222$. As in the case of **7**, $[\{Ni_4(bptz)_4(CH_3CN)_8\}\subset BF_4]^{7+}$ has point symmetry 222 but with a $[BF_4]^-$ ion located on the special position where the three 2-fold rotation axes coincide. The combination of these symmetry elements results in two $[BF_4]^-$ disorder components. The $[PF_6]^-$ ion is also located at a special position and is disordered. The asymmetric unit contains the fragment PF_3, and the 2-fold rotation axes at this special position resulted in two $[PF_6]^-$ disorder components. The four B−F bond distances and the four F−B−F angles of each $[BF_4]^-$ component, as well as the P−F bond distances and the angles F−P−F of each $[PF_6]^-$ component, were restrained to similar values. Similarity restraints rather than distance restraints were used to confirm the identity of the anions from the refined distances. The $[BF_4]^-$ and $[PF_6]^-$ disorder components exhibited tetrahedral and octahedral geometry after least-squares refinement, respectively. The refined distances B−F = 1.42(1) Å and P−F = 1.64(1) Å were found to be slightly longer than those typically observed for $[BF_4]^-$ and $[PF_6]^-$ ions, presumably due to disorder.

[{Ni$_4$(bptz)$_4$(CH$_3$CN)$_4$(H$_2$O)$_4$}⊂ClO$_4$](IO$_4$)$_7$·3CH$_3$CN (9·3CH$_3$CN). Crystals were obtained by layering an acetonitrile solution of **2** over a methanol solution of [n-Bu$_4$N][IO$_4$]. These crystals belong to the monoclinic system, space group $C2/c$. All seven $[IO_4]^-$ anions were disordered. For each anion, two components were defined with 50% site occupancies; the I−O distances and O−I−O angles were constrained to have similar values. The $[ClO_4]^-$ inside the cavity of the square was also disordered and was modeled using two components and restraints on the Cl−O and O···O distances. The site occupancies of each component, derived from the final refinement, are 0.325(2) and 0.675(2). As previously done, constraints were used so that the two residues of each disorder component would have the same displacement parameters. Due to the complexity of the disorder model, several atoms that belong to disordered groups were refined isotropically during the final cycles of refinement.

[{Ni$_4$Br$_7$(bptz)$_4$(CH$_3$CN)}⊂Br$_3$]·2CH$_3$CN·2.5C$_7$H$_8$ (10·2CH$_3$CN·2.5C$_7$H$_8$). Crystals were grown by diffusing a 1:2 dichloromethane/toluene solution of [n-Bu$_4$N][Br$_3$] into an acetonitrile solution of **2** in a 0.5 mm sealed glass tube. Disordered interstitial toluene molecules were located, but it was difficult to establish their exact site occupancies from the X-ray data. The structure was solved and refined in the space group $P2_1/n$. One toluene molecule resides on an inversion center, which leads to a phenyl ring that appears to be substituted at both positions 1 and 4. The C(19S)−C(20S) and C(20S)−C(21S) distances of the toluene molecule were restrained. Due to the complexity of the disorder model, and the diffuse nature of the peaks in the interstices of the crystal, all atoms of the solvent molecules were refined isotropically during the final cycles of refinement.

[Ni$_2$(bptz)(CH$_3$CN)$_8$][ClO$_4$]$_4$ (11). Crystals of **11** were obtained by layering the reaction filtrate obtained after isolation of compound **2** with diethyl ether. The structure was solved and refined in the space group $P\bar{1}$. Two of the $[ClO_4]^-$ anions were disordered and appropriately modeled. All non-hydrogen atoms were refined anisotropically.

{[Mn(bptz)(CH$_3$CN)$_2$][BF$_4$]$_2$·1.5CH$_3$CN}$_\infty$ (12·1.5CH$_3$CN). The structure was solved and refined in the space group $P\bar{1}$. One $[BF_4]^-$ anion and one acetonitrile molecule were disordered and appropriately modeled. The disordered CH_3CN is located on an inversion center. The bond distances and angles of the components used to describe the disorder were restrained to chemically reasonable values. In the final cycles of refinement, all non-hydrogen and non-disordered atoms were refined anisotropically.

(20) Sheldrick, G. M. *SHELXS-97. A Program for Crystal Structure Solution*; University of Göttingen: Göttingen, Germany, 1997. Sheldrick, G. M. *SHELXL-97. A Program for Crystal Structure Refinement*; University of Göttingen: Göttingen, Germany, 1997.
(21) (a) Spek, A. L. *PLATON*; University of Utrecht: The Netherlands, 2001. (b) Spek, A. L. *Acta Crystallogr.* **1990**, *A46*, 194.
(22) Nardelli, M. *PARST. J. Appl. Crystallogr.* **1995**, *28*, 659.
(23) Flack, H. D. *Acta Crystallogr.* **1983**, *A39*, 876.

Table 1. Crystal and Structural Refinement Data for **1**·4CH_3CN, **2**·4CH_3CN·C_4H_8O, **3**·4CH_3CN, **5**·2CH_3CN, **7**, **8**, **9**·3CH_3CN, **10**·2CH_3CN·2.5$C_6H_5CH_3$, **11**, and **12**·1.5CH_3CN

	1·4CH_3CN	**2**·4CH_3CN·C_4H_8O	**3**·4CH_3CN	**5**·2CH_3CN	**7**	**8**	**9**·3CH_3CN	**10**·2CH_3CN·2.5$C_6H_5CH_3$	**11**	**12**·1.5CH_3CN
formula	$Ni_4C_{72}N_{36}B_8F_{32}H_{68}$	$Ni_4C_{76}N_{36}Cl_8O_{33}H_{76}$	$Zn_4C_{72}N_{36}B_8F_{32}H_{68}$	$Ni_5N_{42}Sb_{10}F_{60}C_{84}H_{76}$	$Ni_4C_{64}N_{32}Sb_7F_{42}IH_{56}$	$Ni_4C_{64}N_{32}BF_{46}Sb_6PH_{56}$	$Ni_4C_{62}N_{31}O_{36}I_7ClH_{61}$	$Ni_4C_{71.5}N_{27}Br_{10}H_{61}$	$Ni_2C_{28}N_{14}Cl_4O_{16}H_{32}$	$MnC_{19}N_{9.5}B_2F_8H_{18.5}$
formula weight	2366.94	2540.17	2393.58	4324.92	3285.4	3154.53	2975.01	2332.41	1079.90	608.49
temp (K)	110(2)	110(2)	110(2)	110(2)	110(2)	110(2)	110(2)	110(2)	110(2)	110(2)
crystal system	triclinic	monoclinic	triclinic	monoclinic	orthorhombic	orthorhombic	monoclinic	monoclinic	triclinic	triclinic
space group	$P\bar{1}$ (No. 2)	$P2_1/n$ (No. 14)	$P\bar{1}$ (No. 2)	$C2/c$ (No. 15)	$I222$ (No. 23)	$I222$ (No. 23)	$C2/c$ (No. 15)	$P2_1/n$ (No. 14)	$P\bar{1}$ (No. 2)	$P\bar{1}$ (No. 2)
a (Å)	14.118(3)	15.082(3)	13.924(1)	17.933(4)	18.145(4)	17.869(4)	20.358(4)	13.197(3)	8.639(5)	9.135(2)
b (Å)	17.090(3)	31.922(6)	17.071(1)	28.314(6)	14.925(3)	14.762(3)	17.493(4)	27.700(6)	10.856(5)	10.859(2)
c (Å)	21.774(4)	22.305(5)	21.940(1)	29.459(6)	22.529(4)	22.326(4)	28.123(6)	23.557(5)	12.362(5)	14.631(3)
α (°)	94.87(3)	90	94.46(1)	90	90	90	90	90	98.355(5)	99.48(3)
β (°)	91.43(3)	104.11(3)	92.51(1)	104.82(3)	90	90	98.53(3)	100.45(3)	104.675(5)	107.53(3)
γ (°)	97.47(3)	90	97.79(1)	90	90	90	90	90	97.317(5)	102.27(3)
V (Å^3)	5187(2)	10415(4)	5143.5(5)	14460(5)	6101(2)	5889(2)	9904(3)	8469(3)	1093.2(9)	1311(1)
crystal description	block	plate	plate	prism	block	plate	rectangular plate	plate	needle	plate
color	green	brown	orange	green	brown	brown	brown	brown	green	orange
crystal size (mm^3)	0.5 × 0.2 × 0.1	0.9 × 0.7 × 0.1	0.3 × 0.1 × 0.05	0.20 × 0.13 × 0.05	0.88 × 0.68 × 0.31	0.73× 0.41 × 0.28	0.20 × 0.10 × 0.06	0.44 × 0.26 × 0.05	0.41 × 0.23 × 0.10	0.30 × 0.18 × 0.15
Z	2	4	2	4	2	2	4	4	1	1
ρ_{calc} (g/cm^3)	1.516	1.620	1.545	1.987	1.788	1.779	1.995	1.829	1.640	1.541
μ (mm^{-1})	0.831	1.014	1.039	2.600	2.488	2.112	3.053	5.652	1.188	0.589
F(000)	2384	5184	2400	8256	3128	3032	5752	4564	550	612
θ range (°)	1.46−24.71	1.97−28.36	1.21−28.33	1.38−24.71	1.77−27.13	1.46−24.71	1.64−24.71	1.15−25.72	4.21−25.49	2.37−24.71
diffraction limits (h, k, l)	$-15 < h < 16$ $-20 < k < 19$ $-25 < l < 12$	$-19 < h < 17$ $-42 < k < 42$ $-27 < l < 29$	$-18 < h < 18$ $-22 < k < 22$ $-28 < l < 28$	$-21 < h < 19$ $-30 < k < 33$ $-29 < l < 34$	$-22 < h < 23$ $-19 < k < 19$ $-24 < l < 28$	$-16 < h < 21$ $-17 < k < 17$ $-26 < l < 26$	$-16 < h < 23$ $-20 < k < 20$ $-33 < l < 33$	$-12 < h < 16$ $-33 < k < 26$ $-28 < l < 28$	$-10 < h < 7$ $-10 < k < 12$ $-14 < l < 14$	$-10 < h < 10$ $-12 < k < 12$ $-17 < l < 17$
reflections collected	24784	79349	62932	36480	22697	17435	34889	43302	4421	12767
independent reflections	16454 [R(int) = 0.0434]	25377 [R(int) = 0.1143]	24556 [R(int) = 0.0545]	12303 [R(int) = 0.0372]	6678 [R(int) = 0.0554]	5005 [R(int) = 0.0829]	8369 [R(int) = 0.0923]	15992 [R(int) = 0.1422]	3362 [R(int) = 0.0349]	4445 [R(int) = 0.0802]
completeness to θ_{max} (%)	92.9	97.5	95.7	99.7	98.9	99.4	99.2	99.0	82.6	99.2
data/param/restraints	16454/1365/92	25377/1430/128	24556/1361/77	12303/1179/169	6678/331/32	5005/358/49	8369/654/73	15992/859/17	3362/310/15	4445/382/41
R,[a] wR[b] [$I > 2\sigma(I)$]	0.087, 0.206	0.058, 0.126	0.070, 0.191	0.108, 0.316	0.066, 0.163	0.081, 0.209	0.109, 0.280	0.065, 0.147	0.061, 0.141	0.053, 0.113
R,[a] wR[b] (all data)	0.154, 0.243	0.194, 0.161	0.134, 0.237	0.143, 0.343	0.076, 0.169	0.111, 0.231	0.192, 0.345	0.209, 0.205	0.128, 0.179	0.122, 0.139
goodness-of-fit[c] (F^2)	1.030	0.860	1.048	1.303	0.909	1.040	1.064	0.956	0.973	0.907
largest diff. peak, hole (e Å^{-3})	1.19, −0.95	1.40, −1.15	1.97, −2.57	6.34, −2.91	2.08, −2.61	1.74, −0.83	2.93, −2.52	1.38, −0.98	0.68, −0.61	0.33, −0.50

[a] $R = \sum||F_o| - |F_c||/\sum|F_o|$. [b] $wR = \{\sum[w(F_o^2 - F_c^2)^2]/\sum w(F_o^2)^2]\}^{1/2}$. [c] Goodness-of-fit = $\{\sum[w(F_o^2 - F_c^2)^2]/(n - p)\}^{1/2}$, where n is the number of reflections and p is the total number of parameters refined.

Results

Synthesis and Stability Studies of the Cyclic Cations. The Ni(II) cation reacts with bptz in CH_3CN to form products of nuclearity three, four, or five depending on the anions present in solution. In accord with the structural similarity of the products to polygons, they are referred to as molecular triangles, squares, and pentagons. Reactions of $[Ni(CH_3CN)_6][BF_4]_2$ or $Ni(ClO_4)_2 \cdot 6H_2O$ with bptz in a 1:1 molar ratio in CH_3CN afford high yields of the partially solvated $[Ni_4]^{8+}$ molecular squares of the type $[\{Ni_4(bptz)_4(CH_3CN)_8\}\subset X]^{7+}$ ($X = [BF_4]^-$ (**1**), $[ClO_4]^-$ (**2**), respectively) (Scheme 1). The structure of **1** with a $[BF_4]^-$ anion located inside the cavity has already been reported.[13a] Analogous results are obtained with the Zn(II) ion; reactions of $[Zn(CH_3CN)_4][BF_4]_2$ or $Zn(ClO_4)_2 \cdot 6H_2O$ with bptz in a 1:1 molar ratio afford molecular squares of the type $[\{Zn_4(bptz)_4(CH_3CN)_8\}\subset X]^{7+}$ ($X = [BF_4]^-$ (**3**), $[ClO_4]^-$ (**4**), respectively) (Scheme 1).[24] In both cases, the single crystal X-ray structural determinations revealed that the anions are encapsulated in the tetranuclear cation cavities, as found for the Ni(II) analogues.

Scheme 1

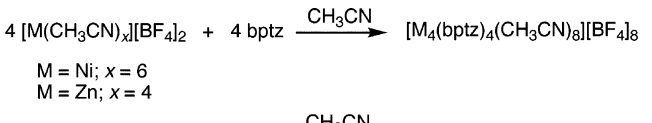

Scheme 2

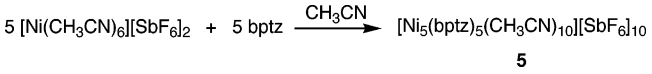

The $[Ni_4]^{8+}$ cations are stable under a variety of conditions, as evidenced by the fact that, regardless of the ratio of bptz to Ni(II) salts (up to 10:1), the reactions proceed in acetonitrile at room temperature to afford molecular squares. If the reactions are refluxed for one week, the same products are obtained in nearly quantitative yields. Identical reactions performed in acetone or nitromethane, in the presence of the same anions, also yield the cyclic $[Ni_4(bptz)_4(CH_3CN)_8]^{8+}$ cations, as evidenced by mass spectrometric data (vide infra), but alcohols and water hinder the formation of the squares.

The reaction of $[Ni(CH_3CN)_6][SbF_6]_2$ with bptz in 1:1 ratio in acetonitrile affords the pentagon $[Ni_5(bptz)_5(CH_3CN)_{10}][SbF_6]_{10}$ (**5**) (Scheme 2) with one $[SbF_6]^-$ ion encapsulated in the cation cavity, as determined by a single crystal X-ray structural determination of the product.[13b] As in the case of the squares **1**−**4**, the $[\{Ni_5(bptz)_5(CH_3CN)_{10}\}\subset SbF_6]^{9+}$ unit persists in solution even after one week of reflux, as confirmed by mass spectrometric and X-ray crystallographic studies (vide infra). The use of different ratios of bptz to $[Ni(CH_3CN)_6][SbF_6]_2$ does not affect the identity of the product, but results in lower yields.

Alternatively, the reaction of $[Ni(CH_3CN)_6][NO_3]_2$ with bptz in a 1:1 ratio produces an insoluble yellow solid, **6**. IR spectroscopic data of **6** confirmed the presence of bptz and nitrate anions with no evidence of coordinated acetonitrile molecules. The same product is obtained by treating **5** with $[n\text{-}Bu_4N][NO_3]$ in acetonitrile. Electrospray mass spectrometric studies indicate that compound **6** is trinuclear, the only instance in which this nuclearity was observed in solution (vide infra). Despite numerous efforts, structural information for this species could not be obtained in the solid state due to the lack of suitable single crystals. Likewise, efforts to obtain single crystals from the reaction of $[Ni(CH_3CN)_6][CF_3SO_3]_2$ with bptz were unsuccessful, which may be attributed to the size and shape of $[CF_3SO_3]^-$, making it an unsuitable template for cyclic oligomers.

Interconversion between the $[Ni_5]^{10+}$ and $[Ni_4]^{8+}$ Cyclic Cations. The role of the anion in dictating the preferred metallacyclophane of the bptz/metal reactions is evident. Small anions with similar shapes,[25] such as $[BF_4]^-$ and $[ClO_4]^-$, yield the squares **1**−**4**, whereas the larger anion $[SbF_6]^-$ favors the pentagon **5**. The possibility of transforming the $[Ni_5]^{10+}$ core into $[Ni_4]^{8+}$ was tested by treating a pure sample of **5** with an excess of $[BF_4]^-$ anions (Scheme 3). Crystals were obtained from an acetonitrile solution of **5**, which had been layered over a saturated benzene solution of $[n\text{-}Bu_4N][BF_4]$. Indexing of the X-ray data confirmed that the crystal exhibits the same unit cell dimensions as **1**.[13a] Accordingly, addition of excess $[n\text{-}Bu_4N][ClO_4]$ to a sample of **5** and subsequent recording of the mass spectrum leads to the conclusion that complete conversion of the pentagon to the square takes place (Scheme 3; vide infra).

Scheme 3

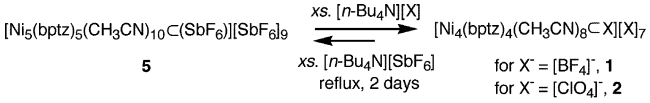

Scheme 4

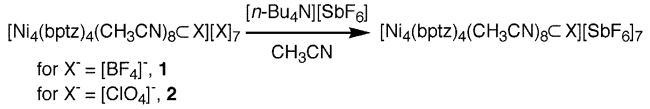

It was found, however, that the transformation of the molecular squares to the pentagon is not as facile as the reverse transformation. A solution of **1** or **2** dissolved in acetonitrile and layered over a saturated solution of $[n\text{-}Bu_4N][SbF_6]$ in toluene affords crystals of the molecular square only, with encapsulated $[BF_4]^-$ or $[ClO_4]^-$ anions and $[SbF_6]^-$ located in the interstices (Scheme 4). Under more forcing conditions, i.e., addition of a large excess of $[n\text{-}Bu_4N][SbF_6]$ to a solution of **1** in acetonitrile (ratio > 50:1) with reflux for 2 days, a partial transformation of the square to the pentagon takes place (Scheme 3), as evidenced by mass spectrometric studies of the resulting solution (vide infra). The fact that the transformation of the pentagon into the square (Scheme 3) takes place under milder conditions provides convincing evidence that the square is more stable than its pentagon counterpart.

The relative instability of the pentagon **5** was capitalized upon for the synthesis of other square derivatives with the aim of probing the template effects of various anions. In one reaction, a solution of **5** was treated with excess $[n\text{-}Bu_4N][I]$, which resulted in the instantaneous precipitation of a brown solid. After the initial insoluble solid was removed by filtration, the remaining light brown solution was treated with toluene to yield crystals of $[\{Ni_4(bptz)_4(CH_3CN)_8\}\subset I][SbF_6]_7$ (**7**), which were

(24) A previous report in the literature describes the synthesis and molecular structure of $[Zn_4(bptz)_4(H_2O)_4(CH_3CN)_4][ClO_4]_8 \cdot 2CHCl_3 \cdot 4CH_3CN$: Bu, X.-H.; Morishita, H.; Tanaka, K.; Biradha, K.; Furusho, S.; Shionoya, M. *Chem. Commun.* **2000**, 971.

(25) Mingos, D. M. P.; Rohl, A. L. *Inorg. Chem.* **1991**, *30*, 3769.

Scheme 5

$$[Ni_5(bptz)_5(CH_3CN)_{10}\subset(SbF_6)][SbF_6]_9 \xrightarrow{xs.\ [n\text{-}Bu_4N][I]} [Ni_4(bptz)_4(CH_3CN)_8\subset I][SbF_6]_7$$

5 **7**

Scheme 6

$$[Ni_4(bptz)_4(CH_3CN)_8\subset I][SbF_6]_7 \xrightarrow{TlPF_6} [Ni_5(bptz)_5(CH_3CN)_{10}\subset(SbF_6)][SbF_6]_x[PF_6]_{9-x}$$

7 $x = 3$ or 4

Tl[I]

Scheme 7

$$[Ni_5(bptz)_5(CH_3CN)_{10}\subset(SbF_6)][SbF_6]_9 \xrightarrow{[n\text{-}Bu_4N][BF_4]/[n\text{-}Bu_4N][PF_6]} [Ni_4(bptz)_4(CH_3CN)_8\subset(BF_4)][PF_6][SbF_6]_6$$

5 **8**

found to contain an iodide anion in the cavity of the square (Scheme 5). Attempts to synthesize this compound by using NiI_2 as the source of Ni(II) led to an insoluble, presumably polymeric material.

The species $[\{Ni_4(bptz)_4(CH_3CN)_8\}\subset I][SbF_6]_7$ was used to examine the stability of the square in the absence of square templating ions. Abstraction of the encapsulated iodide with $TlPF_6$ leads to transformation of the square to the less stable pentagon (Scheme 6) because apparently no appropriate square templating anion is present. The identity of the product in Scheme 6 was confirmed by single crystal X-ray crystallographic studies of independent crystals (different crystals contain various amounts of $[PF_6]^-$ and $[SbF_6]^-$ outer-sphere anions).

The effect of size, shape, and geometry of the anion on the formation of a particular cyclic product was further probed by layering a solution of **5** with an equimolar mixture of $[n\text{-}Bu_4N][BF_4]$ and $[n\text{-}Bu_4N][PF_6]$, which resulted in the isolation of **8** (Scheme 7). In **8**, a $[BF_4]^-$ ion is located inside the molecular square, presumably because $[SbF_6]^-$ and $[PF_6]^-$ anions lack the appropriate size (they are too large) and shape[25] to occupy the square cavity. Microanalytical data collected on independent batches of the product indicated that different amounts of $[PF_6]^-$ and $[SbF_6]^-$ outer-sphere anions are incorporated in the crystals.

Exchange of the Encapsulated Anion in $[\{Ni_4(bptz)_4(CH_3CN)_8\}\subset ClO_4][ClO_4]_7$. From the aforementioned results, it is obvious that anions such as $[BF_4]^-$ and $[ClO_4]^-$ assist in the formation of stable molecular squares (Scheme 1). A natural question that arises is how important are both the encapsulated and outer-sphere anions to the overall stability of the squares. Addition of a large excess of $[n\text{-}Bu_4N][IO_4]$ to a solution of $[\{Ni_4(bptz)_4(CH_3CN)_8\}\subset ClO_4][ClO_4]_7$ (**2**) resulted in the isolation of crystals of $[\{Ni_4(bptz)_4(CH_3CN)_4(H_2O)_4\}\subset ClO_4][IO_4]_7$ (**9**) (Scheme 8). Although the solution was saturated with $[IO_4]^-$, the isolated compound still contains a $[ClO_4]^-$ anion inside the cavity and only the outer-sphere anions have been replaced with periodate anions. Analogous reactions with Br^- ions proceed with rapid formation of an insoluble product rather than crystals. Slow diffusion of an acetonitrile solution of **2** into a dichloromethane/toluene solution of $[n\text{-}Bu_4N][Br_3]$, however, yields crystals of the formally neutral molecule $[\{Ni_4(bptz)_4Br_7(CH_3CN)\}\subset Br_3]$ (**10**) with a $[Br_3]^-$ ion encapsulated in the cavity (Scheme 9).

NMR Spectroscopic Studies. The aromatic region of the ^1H NMR spectrum of $[Zn_4(bptz)_4(CH_3CN)_8][BF_4]_8$ in CD_3CN-d_3 (Figure 1a) exhibits four sets of resonances, which indicates that each bptz ligand is bridging two metal centers in a symmetric fashion. The resonances at δ 8.10, 8.31, 8.52, and

Scheme 8

$$[Ni_4(bptz)_4(CH_3CN)_8\subset(ClO_4)][ClO_4]_7 \xrightarrow{xs.\ [n\text{-}Bu_4N][IO_4]} [Ni_4(bptz)_4(CH_3CN)_4(H_2O)_4\subset(ClO_4)][IO_4]_7$$

2 **9**

Scheme 9

$$[Ni_4(bptz)_4(CH_3CN)_8\subset(ClO_4)][ClO_4]_7 \xrightarrow{xs.\ [n\text{-}Bu_4N][Br_3]} [Ni_4(bptz)_4Br_7(CH_3CN)\subset Br_3]$$

2 **10**

9.25 ppm are ascribed to the 3,3′, 5,5′, 4,4′, and 6,6′ protons of the bptz pyridyl rings in $[Zn_4(bptz)_4(CH_3CN)_8][BF_4]_8$, respectively (Figure 1a). Unbound bptz exhibits resonances at δ 8.64

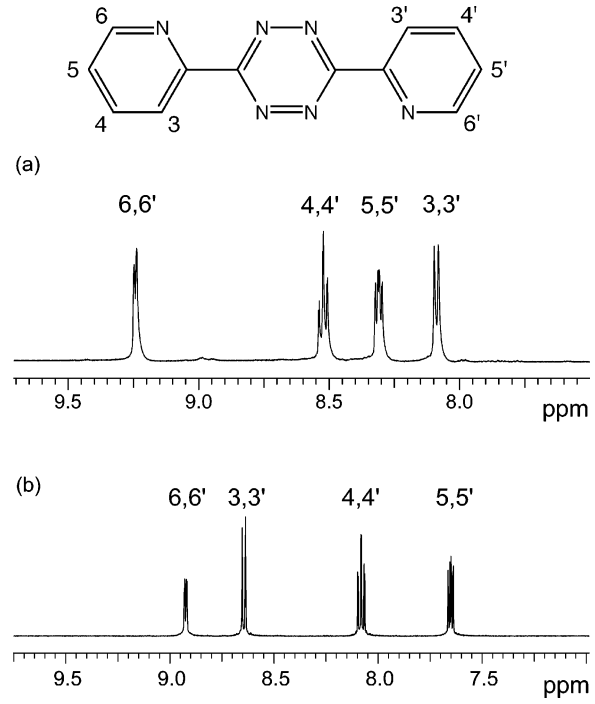

Figure 1. Aromatic region of the ^1H NMR spectrum of (a) $[Zn_4(bptz)_4(CH_3CN)_8][BF_4]_8$ and (b) bptz, in CD_3CN-d_3 at room temperature.

(3,3′), 7.65 (5,5′), 8.10 (4,4′), and 8.93 (6,6′) ppm for the corresponding protons in CD_3CN-d_3 (Figure 1b). The resonance (doublet) for protons 6,6′-H of $[Zn_4(bptz)_4(CH_3CN)_8][BF_4]_8$, which are adjacent to the metal binding sites, is shifted downfield by $\Delta\delta$ 0.33 ppm with respect to the corresponding free bptz protons due to the inductive effect of the metal.[26] Likewise, the resonances for protons 5,5′-H and 4,4′-H shift downfield by $\Delta\delta$ 0.66 and 0.42 ppm, respectively, and show multiplet splitting due to three-bond coupling to neighboring protons on the same ring. Conversely, the resonance (doublet) for 3,3′-H is shifted upfield by $\Delta\delta$ 0.54 ppm with respect to 3,3′-H of free bptz; this upfield shift is ascribed to the shielding of hydrogen atoms 3,3′-H, due to their close proximity to the pyridyl ring of the neighboring bptz unit.[27] Consideration of the relative positions of these protons in **3** indicates that the distances from 3,3′-H to the centroid of the shielding pyridyl rings are 3.913 and 4.338 Å, respectively (for comparison, 4,4′-H are at 5.819 and 6.262 Å from the pyridyl ring centroid of the neighboring bptz unit).

(26) (a) Dijt, F. J.; Canters, G. W.; den Hartog, J. H. J.; Marcelis, A. T. M.; Reedijk, J. *J. Am. Chem. Soc.* **1984**, *106*, 3644. (b) Kong, P. C.; Theophanides, T. *Inorg. Chem.* **1974**, *13*, 1981.
(27) (a) Ting, Y.; Lai, Y.-H. *J. Am. Chem. Soc.* **2004**, *126*, 909. (b) Burgeson, J. R.; Renner, M. K.; Hardt, I.; Ferrence, G. M.; Standard, J. M.; Hitchcock, S. R. *J. Org. Chem.* **2004**, *69*, 727.

Gradual addition of a $[Zn(CH_3CN)_4][BF_4]_2$ solution in CD_3CN-d_3 to a bptz solution in CD_3CN-d_3 at room temperature leads to a broadening and shifting of all the bptz proton resonances, which suggests that rapid chemical exchange is occurring.[36] A ^1H NMR spectrum identical to that of the isolated complex $[Zn_4(bptz)_4(CH_3CN)_8][BF_4]_8$ in CD_3CN-d_3 (Figure 1a) is not acquired until the molar ratio Zn(II):bptz is 3:4. The addition of excess $[Zn(CH_3CN)_4][BF_4]_2$, however, does not affect the ^1H NMR spectrum of the isolated complex $[Zn_4(bptz)_4(CH_3CN)_8][BF_4]_8$ in CD_3CN-d_3. Moreover, the ^1H NMR spectrum of the reaction solution of $[Zn(CH_3CN)_4][SbF_6]_2$ with bptz in a 1:1 ratio in CD_3CN-d_3 does not contain any resonances that can be attributed to the presence of the square $[Zn_4(bptz)_4(CH_3CN)_8]^{8+}$ in solution unless $NaBF_4$ is added, a fact which underscores the importance of the appropriate anion for stabilizing a specific cyclic structure.

The ^{19}F NMR spectrum of $[Zn_4(bptz)_4(CH_3CN)_8][BF_4]_8$ in CD_3CN-d_3 at +22 °C exhibits one resonance at δ −151 ppm, which is ascribed to the free $[BF_4]^-$ ions.[28,29] The ^{19}F NMR spectrum of $[Zn(CH_3CN)_4][BF_4]_2$ in CD_3CN-d_3 also exhibits a resonance at δ −151 ppm, due to the free $[BF_4]^-$ ions. Due to coupling of ^{11}B and ^{10}B to the ^{19}F nuclei, the ^{19}F resonance of $[Zn_4(bptz)_4(CH_3CN)_8][BF_4]_8$ at room temperature is split into two peaks in the relative ratio of ∼4:1, corresponding to the natural abundance of ^{11}B to ^{10}B;[30] the two distinct maxima of the ^{19}F NMR resonance for the $[BF_4]^-$ ions collapse at temperatures below −5 °C.[30]

The ^{19}F NMR spectrum of $[Zn_4(bptz)_4(CH_3CN)_8][BF_4]_8$ in CD_3CN-d_3 exhibits a single resonance at δ −151 ppm in the temperature range −10 to +70 °C (the collapse of the $^{10}B-^{11}B$ isotope shift at high temperatures in the ^{19}F NMR spectra of **3** in CD_3CN-d_3 is attributed to the exchange of fluorine among boron atoms[30]), but at −10 °C, a second ^{19}F resonance of lower intensity appears at δ −144 ppm. The latter resonance is ascribed to the encapsulated $[BF_4]^-$ ions in the cavity of the square, exchanging slowly with the free $[BF_4]^-$ ions on the NMR time scale at this temperature. The identity of this peak is also supported by its consistent appearance in the ^{19}F NMR spectra of dissolved crystals of $[Zn_4(bptz)_4(CH_3CN)_8][BF_4]_8$ in CD_3CN-d_3 and its downfield position relative to free $[BF_4]^-$ ions (the magnetically shielded zone of the cavity shifts the ^{19}F NMR resonances of the encapsulated ions to lower field[31]),[28,29,32] as well as its $\Delta\delta(^{19}F)$ ∼7 ppm with respect to the free $[BF_4]^-$ ions, which is comparable to the $\Delta\delta(^{19}F)$ of other systems with free and encapsulated $[BF_4]^-$ ions.[32] The resonance at δ −144 ppm persists at lower temperatures, but spectra could not be acquired at temperatures below −42 °C due to the freezing point of CD_3CN-d_3.

IR Spectroscopy. Notable features of the IR spectra of **1**, **2**, and **5** include two ν(C≡N) bands in the range 2318−2325 cm^{-1}, corresponding to the stretching modes of the coordinated acetonitrile ligands. Sharp bands at 1064 and 1054 cm^{-1} in the IR spectra of **1** and **3**, respectively, are attributed to the ν(B−F) stretching mode of the tetrafluoroborate anions.[33] Analogous ν(Cl−O) stretches of the perchlorate ions[33] are observed at 1098 cm^{-1} for compounds **2** and **4**. The expected ν(C≡N) stretches for the coordinated acetonitrile molecules in **3** and **4** were not observed, however, which may be due to prolonged pumping of the samples leading to the loss of the ligands in the solid state. An alternative explanation is that these stretching modes are too weak to be observed.[34] IR spectroscopic data of **6** did not reveal any ν(C≡N) modes for coordinated CH_3CN ligands. It is inferred, however, due to bands in the range 1000−1500 cm^{-1},[33] that the nitrate groups are chelating to the Ni(II) ions in addition to acting as outer-sphere anions.

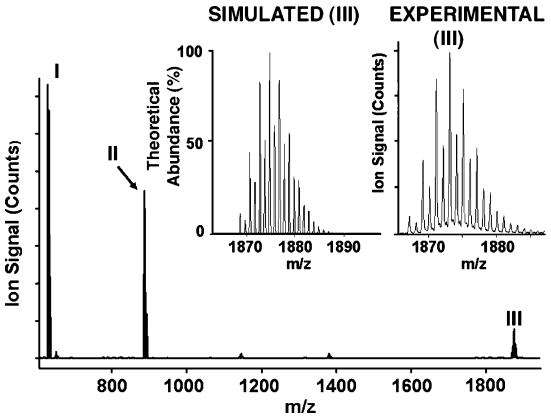

Figure 2. Electrospray mass spectrum of $[\{Ni_4(bptz)_4(CH_3CN)_8\}\subset ClO_4]-[ClO_4]_7$ (**2**) in CH_3CN. The ion signals displayed correspond to $[Ni_4(bptz)_4(ClO_4)_7 + 2H]^{3+}$ (**I**) at *m*/*z* 625.9, $[Ni_4(bptz)_4(ClO_4)_6]^{2+}$ (**II**) at *m*/*z* 888.2, and $[Ni_4(bptz)_4(ClO_4)_7]^+$ (**III**) at *m*/*z* 1875.8 (parent ion peak). The experimental and theoretical isotopic distribution patterns of **III** are shown in the inset.

Electrospray Mass Spectroscopic Studies. For compound **2**, the ion signal at *m*/*z* 1875.8 is assigned to the parent ion $[Ni_4(bptz)_4(ClO_4)_7]^+$ (Figure 2). The experimental and theoretical isotopic distribution patterns are identical. Ion signals were also observed for $[Ni_4(bptz)_4(ClO_4)_6]^{2+}$ and $[Ni_4(bptz)_4(ClO_4)_7 + 2H]^{3+}$ at *m*/*z* 888.2 and 625.9, respectively. The mass spectrum of **2** remained unchanged when the solution was left to stand for over a week, which indicates that the $[Ni_4]^{8+}$ square is stable in solution. Compound **4** exhibits an ion signal for $[Zn_4(bptz)_4(ClO_4)_7]^+$ at *m*/*z* 1902.6 (Figure S1), which is indicative of the presence of the molecular square in solution. The ESI-MS spectra of complexes **1** and **3**, i.e., the tetrafluoroborate counterparts of **2** and **4**, showed similar results, but the spectra were complicated by reactions with the anion to give fluoride-containing species.[35]

The mass spectrum of the pentagon **5** exhibits the highest *m*/*z* ion signal at 3596.3 (Figure 3), ascribed to $[Ni_5(bptz)_5(SbF_6)_9]^+$, with no evidence of a $[Ni_4]^{8+}$ species in equilibrium with the pentagon, thus confirming the presence of the intact pentagon cage. Ion signals at *m*/*z* 1060.8 and 1297.6 correspond to $[Ni_2(bptz)(SbF_6)_3]^+$ and $[Ni_2(bptz)(SbF_6)_4 + H]^+$, respectively. Moreover, the nuclearity of complex **5** in the presence of $[NO_3]^-$ anions was probed by mass spectrometry. Addition

(28) Amouri, H.; Rager, M. N.; Cagnol, F.; Vaissermann, J. *Angew. Chem., Int. Ed.* **2001**, *40*, 3636.
(29) Fleming, J. S.; Mann, K. L. V.; Carraz, C.-A.; Psillakis, E.; Jeffrey, J. C.; McCleverty, J. A.; Ward, M. D. *Angew. Chem., Int. Ed.* **1998**, *37*, 1279.
(30) Gillespie, R. J.; Hartman, J. S.; Parekh, M. *Can. J. Chem.* **1968**, *46*, 1601.
(31) Parac, T. N.; Caulder, D. L.; Raymond, K. N. *J. Am. Chem. Soc.* **1998**, *120*, 8003.
(32) Mann, S.; Huttner, G.; Zsolnai, L.; Heinze, K. *Angew. Chem., Int. Ed. Engl.* **1996**, *35*, 2808.
(33) Nakamoto, K. *Infrared and Raman Spectra of Inorganic and Coordination Compounds*; John Wiley: New York, 1997.
(34) Johnson, A.; Taube, H. *J. Indian Chem. Soc.* **1989**, *66*, 503.
(35) While performing mass spectrometric studies on inorganic complexes associated with $[BF_4]^-$ and $[PF_6]^-$ anions, ion peaks that can be assigned only to fluoride adducts, due to their isotopic patterns and molecular masses, are observed.

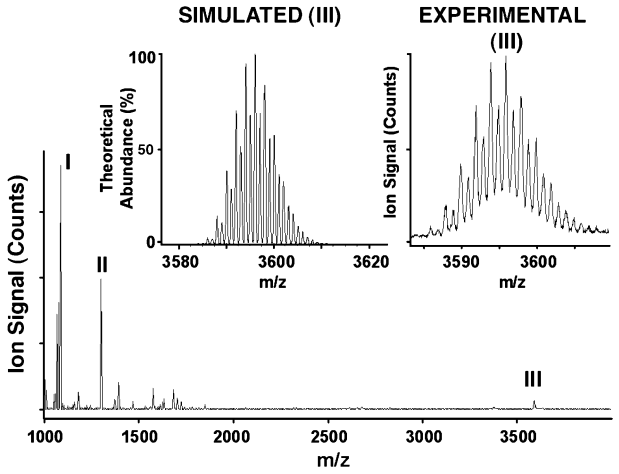

Figure 3. Electrospray mass spectrum of $[\{Ni_5(bptz)_5(CH_3CN)_{10}\}\subset SbF_6][SbF_6]_9$ (**5**) in CH_3CN. The ion signals displayed correspond to $[Ni_2(bptz)(SbF_6)_3]^+$ (**I**) at *m*/*z* 1060.8, $[Ni_2(bptz)(SbF_6)_4 + H]^+$ (**II**) at *m*/*z* 1297.6, and $[Ni_5(bptz)_5(SbF_6)_9]^+$ (**III**) at *m*/*z* 3596.3 (parent ion peak). The experimental and theoretical isotopic distribution patterns of **III** are shown in the inset.

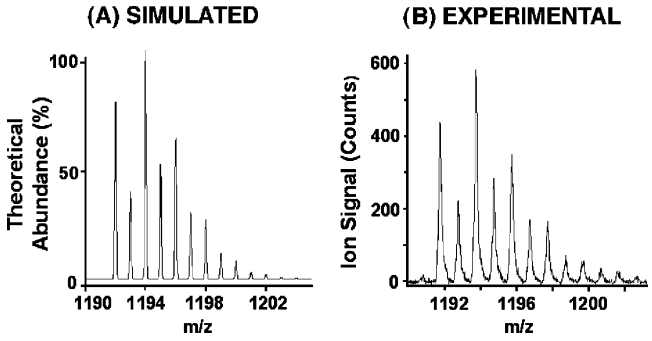

Figure 4. Electrospray mass spectrum of $[Ni_3(bptz)_3][NO_3]_6$ (**6**) in CH_3CN. Parent ion peak for $[Ni_3(bptz)_3(NO_3)_5]^+$ at *m*/*z* 1194.7. (A) Theoretical and (B) experimental isotopic distribution patterns of the parent ion peak.

of excess $[n\text{-}Bu_4N][NO_3]$ to **5** led to the instantaneous precipitation of a yellow solid. After sonication in CH_3CN for 1 h, the sample was subjected to ESI-MS, which revealed an ion signal that corresponds to $[Ni_3(bptz)_3(NO_3)_5]^+$ at *m*/*z* 1194.7 (Figure 4).

The conversion of the $[Ni_5]^{10+}$ species to $[Ni_4]^{8+}$ by addition of an excess of $[ClO_4]^-$ ions, and the reverse reaction of converting $[Ni_4]^{8+}$ to $[Ni_5]^{10+}$ by addition of $[SbF_6]^-$ ions, was monitored by mass spectrometry, and the results were compared to the ESI-MS spectra for isolated crystals of **5** and **2**. Addition of excess $[n\text{-}Bu_4N][ClO_4]$ to complex **5** and subsequent recording of the mass spectrum leads to the conclusion that complete conversion of the pentagon to the square takes place (Scheme 3). The reverse reaction, viz., the transformation of the square to pentagon, does not occur at room temperature. Addition of a large excess of $[n\text{-}Bu_4N][SbF_6]$ to a solution of **2** with subsequent refluxing eventually leads to detectable quantities of $[Ni_5]^{10+}$ cores, but the conversion is not complete even after heating for 5 days (Schemes 3 and 4). In the mass spectrum of the solution of **2** after refluxing for 2 days, ion signals for the species $[Ni_5(bptz)_5(SbF_6)_7 - 2H]^+$, $[Ni_5(bptz)_5(SbF_6)_8 - H]^+$, and $[Ni_5(bptz)_5(SbF_6)_9]^+$ at *m*/*z* 3122.8, 3359.5, and 3596.3, respectively (Figure 5), are observed; these corroborate the formation of the pentagon.

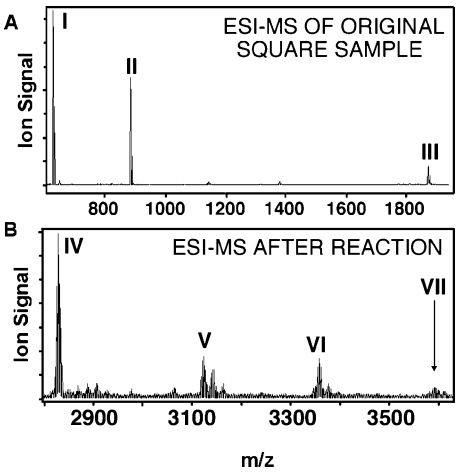

Figure 5. Electrospray mass spectrum of (A) original $[\{Ni_4(bptz)_4(CH_3CN)_8\}\subset ClO_4][ClO_4]_7$ square sample in CH_3CN (the ion signals displayed correspond to $[Ni_4(bptz)_4(ClO_4)_7 + 2H]^{3+}$ (**I**) at *m*/*z* 625.9, $[Ni_4(bptz)_4(ClO_4)_6]^{2+}$ (**II**) at *m*/*z* 888.2, and $[Ni_4(bptz)_4(ClO_4)_7]^+$ (**III**) at *m*/*z* 1875.8 (parent ion peak)) and (B) $[Ni_4(bptz)_4((CH_3CN)_8(ClO_4)_7]^+$ species that has been refluxed with excess $[n\text{-}Bu_4N][SbF_6]$ for 2 days (partial conversion of the square to the pentagon has taken place). Ion signals at *m*/*z* 2829.9, 3122.8, 3359.5, and 3596.3 correspond to the species $[Ni_4(bptz)_4(SbF_6)_7]^+$ (**IV**), $[Ni_5(bptz)_5(SbF_6)_7 - 2H]^+$ (**V**), $[Ni_5(bptz)_5(SbF_6)_8 - H]^+$ (**VI**), and $[Ni_5(bptz)_5(SbF_6)_9]^+$ (**VII**), respectively.

Acetonitrile solutions of $M(ClO_4)_2 \cdot xH_2O$ (M = Mn, Fe, Cu) and bptz in a 1:1 ratio were mixed and their ESI-MS spectra were recorded. In all cases, parent ion signals that correspond to $[M_4(bptz)_4(ClO_4)_7]^+$ for Mn(II), Fe(II), and Cu(II) at *m*/*z* 1860.8 (Figure S2), 1864.5 (Figure S3), and 1895.2 (Figure S4), respectively, were observed. Ion signals corresponding to the loss of one or two bptz ligands from the $[M_4(bptz)_4(ClO_4)_7]^+$ ion are apparent. The parent $[M_4]^{8+}$ species for these particular metal ions are not very stable to the conditions of the ESI-MS experiment, and their ion signals are observed only when the ESI-MS spectrum of a freshly prepared sample is recorded.

To ensure that CH_3CN is the best solvent for promoting the formation of cyclic products with M(II) salts and bptz, a series of mass spectra of the reaction products between $Ni(ClO_4)_2 \cdot 6H_2O$ and bptz in 1:1 ratio were recorded in several different solvents. The results indicate that, in the presence of acetonitrile, acetone, and nitromethane, the square $[Ni_4(bptz)_4(ClO_4)_7]^+$ is formed, whereas protic solvents such as water, ethanol, and methanol are unfavorable for its formation (Figure S5). These findings suggest that the solvent is also a controlling element in the self-assembly of the polygons presented herein.[5]

X-ray Crystallographic Studies. $[\{Ni_4(bptz)_4(CH_3CN)_8\}\subset BF_4][BF_4]_7 \cdot 4CH_3CN$ ($\mathbf{1}\cdot 4CH_3CN$). The essential features of the molecular structure of **1** were reported in a previous communication.[13a] The four pairs of Ni(II) ions and bptz ligands form a molecular square in which each metal ion occupies a vertex and each ligand spans one edge as a bridge between metal centers. The coordination geometry about each Ni(II) ion is distorted octahedral, with four sites being occupied by two different bridging bptz moieties and the two remaining sites being capped by CH_3CN ligands. A plot of the cationic unit $[\{Ni_4(bptz)_4(CH_3CN)_8\}\subset BF_4]^{7+}$ is shown in Figure 6. The four Ni···Ni···Ni vertex angles are in the range of 85.99−93.55°. There is no imposed symmetry on the $[\{Ni_4(bptz)_4$-

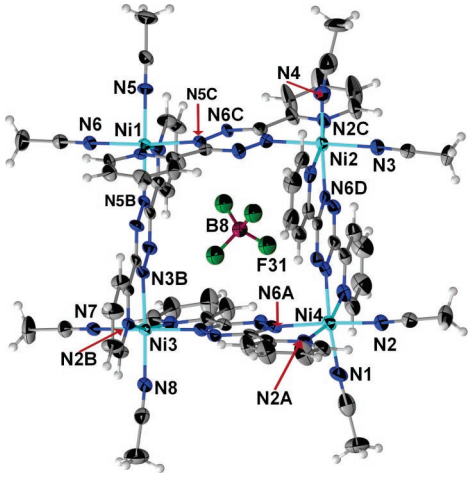

Figure 6. Thermal ellipsoid plot at the 50% probability level of the cationic unit $[\{Ni_4(bptz)_4(CH_3CN)_8\}\subset BF_4]^{7+}$ in **1**·4CH_3CN. Selected bond distances (Å) and angles (°): Ni1−N5 2.031(7), Ni1−N5B 2.097(6), N5C−N6C 1.327(8), N5−Ni1−N5C 86.0(2), N5−Ni1−N5B 173.7(3).

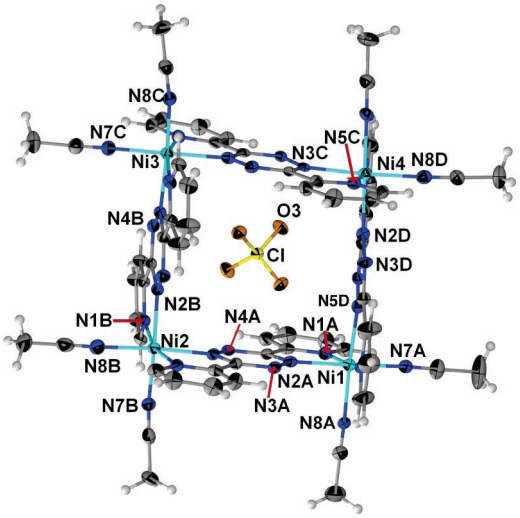

Figure 7. Thermal ellipsoid plot at the 50% probability level of the cationic unit $[\{Ni_4(bptz)_4(CH_3CN)_8\}\subset ClO_4]^{7+}$ in **2**·4CH_3CN·C_4H_8O. Selected bond distances (Å) and angles (°): Ni1−N8A 2.027(5), Ni1−N5D 2.073(5), N2A−Ni1−N8A 90.1(2), N8A−Ni1−N7A 90.6(2), N2A−Ni1−N7A 174.6(2).

$(CH_3CN)_8\}\subset BF_4]^{7+}$ unit; consequently, there are four different Ni···Ni separations, in the range 6.844−6.896 Å. The distances between the centroids of the parallel tetrazine rings are 6.904 and 7.087 Å. The four bptz ligands along the sides of the square create a void space inside the cavity, which is akin to a box with two open faces rather than a square.

$[\{Ni_4(bptz)_4(CH_3CN)_8\}\subset ClO_4](ClO_4)_7$·4$CH_3CN$·$C_4H_8O$ (2·4CH_3CN·C_4H_8O). The molecular structure of **2** is similar to that of the $[BF_4]^-$ salt **1**. A thermal ellipsoid plot of the cationic unit $[\{Ni_4(bptz)_4(CH_3CN)_8\}\subset ClO_4]^{7+}$ is shown in Figure 7. The four Ni···Ni···Ni vertex angles (87.30−92.97°) for this molecular square deviate slightly from being ideal; the average Ni···Ni vertex separation is 6.846 Å. The Ni−N(bptz) bond distances are in the range 2.055(4)−2.112(5) Å. Although the two pyridyl groups of bptz are free to rotate about the C−C bonds between the tetrazine and pyridyl rings, the three rings are nearly coplanar. The distances between the centroids of parallel tetrazine rings are 6.973 and 7.076 Å.

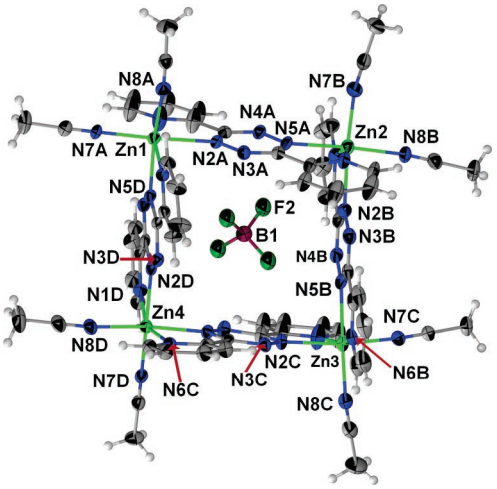

Figure 8. Thermal ellipsoid plot at the 50% probability level of the cationic unit $[\{Zn_4(bptz)_4(CH_3CN)_8\}\subset BF_4]^{7+}$ in **3**·4CH_3CN. Selected bond distances (Å) and angles (°): Zn1−N7A 2.080(4), Zn1−N5D 2.260(4), Zn1−N2A 2.293(4), N8A−Zn1−N7A 92.6(2), N8A−Zn1−N5D 170.6(2), N7A−Zn1−N5D 93.0(2), N8A−Zn1−N2A 89.8(2), N5D−Zn1−N2A 85.9(1).

$[\{Zn_4(bptz)_4(CH_3CN)_8\}\subset BF_4](BF_4)_7$·4$CH_3CN$ (3·4CH_3CN). A thermal ellipsoid plot of the cationic unit $[\{Zn_4(bptz)_4(CH_3CN)_8\}\subset BF_4]^{7+}$ is shown in Figure 8. The molecular structures of complexes **1** and **3** are very similar, but the $[Zn_4]^{8+}$ square is slightly larger than the $[Ni_4]^{8+}$ analogue, with Zn···Zn vertex separations in the range 7.129−7.201 Å. The distances between the centroids of the parallel tetrazine rings are 7.045 and 7.205 Å. The average Zn−N(CH_3CN) distances (2.070−2.091 Å) are shorter than the Zn−N(bptz) distances (2.090−2.284 Å). As in the case of the $[Ni_4]^{8+}$ analogue, a $[BF_4]^-$ anion is located inside the cavity of the Zn(II) square. In addition, an acetonitrile molecule occupies a portion of the cavity volume. The single crystal X-ray structure of the perchlorate salt $[Zn_4(bptz)_4(H_2O)_4(CH_3CN)_4][ClO_4]_8$·2$CHCl_3$·4$CH_3CN$, which crystallized in the chiral space group $C222_1$, has already been reported.[24]

$[\{Ni_5(bptz)_5(CH_3CN)_{10}\}\subset SbF_6][SbF_6]_9$·2$CH_3CN$ (5·2CH_3CN). The essential structural features of **5** were reported in a previous communication.[13b] The thermal ellipsoid plot of the cation $[\{Ni_5(bptz)_5(CH_3CN)_{10}\}\subset SbF_6]^{9+}$ is depicted in Figure 9. The molecular cation consists of a pentagon in which each metal ion occupies a vertex and five bptz ligands span the edges of the polygon. The cavity of $[Ni_5(bptz)_5(CH_3CN)_{10}]^{10+}$ is occupied by a $[SbF_6]^-$ anion and a partially encapsulated CH_3CN molecule. The five Ni···Ni···Ni vertex angles (107.83−108.19°) are close to that of an ideal pentagon (108°), even though the coordination angles N−Ni−N at the vertices are much smaller (91.2(3)−91.7(3)°). Clearly the flexibility of the bptz ligands, which bow inward to compensate for the strain, allows for the formation of the closed pentagon structure.[13b]

$[\{Ni_4(bptz)_4(CH_3CN)_8\}\subset I][SbF_6]_7$ (7). Two significant observations emerged from this single crystal X-ray structural determination, namely that the core structure of the pentagon has been transformed into a square, and that an iodide anion is located inside the cavity. The molecular structure of the cationic unit $[\{Ni_4(bptz)_4(CH_3CN)_8\}\subset I]^{7+}$ is shown in Figure 10. The cation $[\{Ni_4(bptz)_4(CH_3CN)_8\}\subset I]^{7+}$ in **7** has imposed 222 symmetry; therefore, the four Ni···Ni···Ni vertex angles (87.52°) are identical and there are two pairs of Ni···Ni distances (6.785 and 6.839 Å). The $[I]^-$ occupies a smaller molecular square

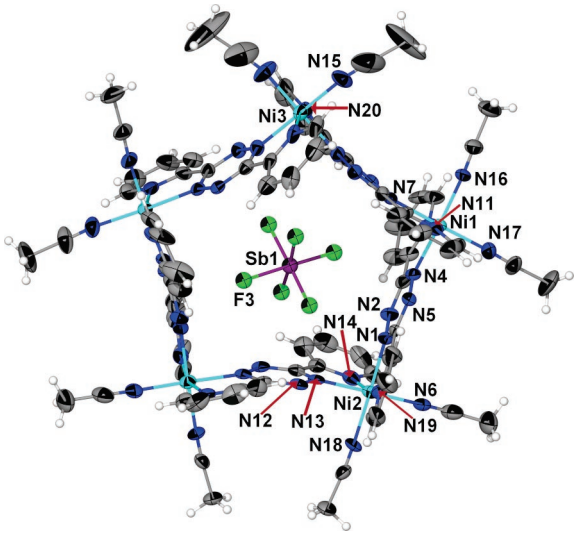

Figure 9. Thermal ellipsoid plot at the 50% probability level of the cationic unit $[\{Ni_5(bptz)_5(CH_3CN)_{10}\}\subset SbF_6]^{9+}$ in **5**·2CH_3CN. Selected bond distances (Å) and angles (°): Ni1−N3 2.085(7), Ni1−N4 2.067(6), Ni1−N7 2.078(7), Ni1−N16 2.039(7), Ni1−N17 2.058(9), N4−Ni1−N7 91.8(3), N3−Ni1−N7 89.1(3), N17−Ni1−N7 176.8(3), N4−Ni1−N3 78.8(3).

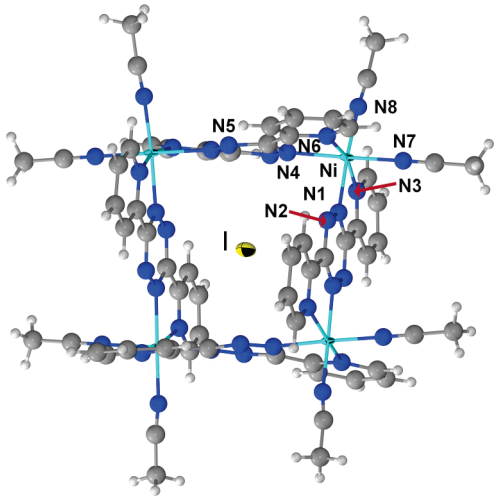

Figure 10. Molecular structure of the cationic unit $[\{Ni_4(bptz)_4(CH_3CN)_8\}\subset I]^{7+}$ in **7**. Thermal ellipsoids are represented at the 50% probability level. The C and N atoms of the bptz ligands are drawn as spheres due to their large thermal parameters. Selected bond distances (Å) and angles (°): Ni−N7 2.045(8), Ni−N1 2.076(6), Ni−N3 2.105(7), N8−Ni−N7 89.5(3), N8−Ni−N6 97.6(3), N8−Ni−N1 174.1(3), N7−Ni−N1 88.73(3), N7−Ni−N3 91.9(3), N6−Ni−N4 77.9(3), N3−Ni−N4 94.6(2).

cavity as compared to the analogous $[BF_4]^-$ and $[ClO_4]^-$ encapsulated cations. The two sets of centroid distances of the parallel tetrazine rings are 6.548 and 7.026 Å. Due to their size, seven outer-sphere $[SbF_6]^-$ anions occupy a large fraction of the unit cell volume. A packing diagram viewed along the *a*-axis is depicted in Figure S6A. It is evident from this diagram that the $[Ni_4(bptz)_4(CH_3CN)_8]^{8+}$ cations are well suited to accommodate I^- ions in the square cavities and that the larger $[SbF_6]^-$ anions result in a gridlike arrangement of squares in the crystal. A much less efficient packing of the squares is evident in the packing diagram of **2** (Figure S6B).

$[\{Ni_4(bptz)_4(CH_3CN)_8\}\subset BF_4][PF_6][SbF_6]_6$ (8). Although crystals of **8** contain three different anions, the compound crystallizes in the same space group as **7** with similar cell dimensions. A thermal ellipsoid plot of $\{[\{Ni_4(bptz)_4(CH_3CN)_8\}\subset BF_4][PF_6]\}^{6+}$ is shown in Figure 11. The cationic unit $[Ni_4(bptz)_4(CH_3CN)_8]^{8+}$ has point symmetry 222, and the four Ni···Ni vertex angles are identical (87.89°), with two pairs of Ni···Ni distances (6.781 and 6.850 Å). The centroid distances of parallel tetrazine rings are 6.393 and 7.066 Å. The crystallographic symmetry site 222 results in two disordered components for the encapsulated $[BF_4]^-$ ion. The $[PF_6]^-$ and $[SbF_6]^-$ ions are located in the interstices created by the cations. As in the case of **7**, the voids formed by the Ni(II) squares are channels rather than simple cavities. The $[BF_4]^-$ ions occupy a portion of the volume inside the channels and are disordered along the channel direction.

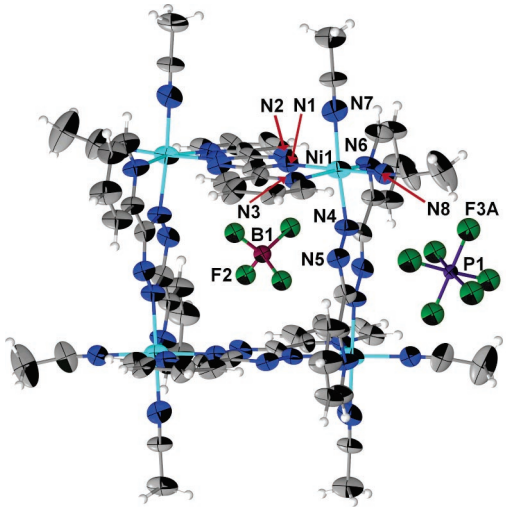

Figure 11. Thermal ellipsoid plot at the 50% probability level of the cationic unit $\{[\{Ni_4(bptz)_4(CH_3CN)_8\}\subset BF_4][PF_6]\}^{6+}$ in **8**. Selected bond distances (Å) and angles (°): Ni1−N1 2.05(1), Ni1−N7 2.07(1), Ni1−N4 2.10(1), Ni1−N6 2.09(1), N8−Ni1−N1 173.2(4), N8−Ni1−N7 91.0(5), N1−Ni1−N7 86.9(5), N1−Ni1−N6 87.8(5), N4−Ni1−N6 77.8(4), N7−Ni1−N3 90.7(5), N4−Ni1−N3 95.8(4).

$[\{Ni_4(bptz)_4(CH_3CN)_4(H_2O)_4\}\subset ClO_4][IO_4]_7\cdot 3CH_3CN$ (9·3CH_3CN). The molecular structure of **9** is typical of the squares encountered in this study. A thermal ellipsoid plot of the $\{[\{Ni_4(bptz)_4(CH_3CN)_4(H_2O)_4\}\subset ClO_4][IO_4]\}^{6+}$ unit is shown in Figure 12. The cation $[Ni_4(bptz)_4(CH_3CN)_8]^{8+}$ resides on a 2-fold axis; thus, there are two pairs of Ni···Ni vertex distances (6.826 and 6.834 Å) and two centroid distances between tetrazine rings of parallel bptz ligands (6.913 and 7.038 Å). The coordination environment of the two pairs of Ni(II) ions is completed by two acetonitrile and two water molecules, respectively. The Ni−O(H_2O) distances are 2.03(1) and 2.04(1) Å. The Ni−N distances are in the same range as for the other Ni−bptz complexes reported herein. It is notable that the $[ClO_4]^-$ anion still occupies the space inside the cavity of the $[Ni_4(bptz)_4(CH_3CN)_8]^{8+}$ square, whereas the outer-sphere anions are $[IO_4]^-$.

$[\{Ni_4(bptz)_4(CH_3CN)Br_7\}\subset Br_3]\cdot 2CH_3CN\cdot 2.5C_7H_8$ (10·2CH_3CN·2.5C_7H_8). The structure of the neutral molecular complex **10** is a square with four Ni(II) ions at the vertices and bptz ligands spanning the edges. This compound is unique among the members of the square series in that it is neutral, if the charge of the encapsulated $[Br_3]^-$ is taken into consideration. A thermal ellipsoid plot of the unit $[\{Ni_4(bptz)_4(CH_3CN)Br_7\}\subset Br_3]$ is illustrated in Figure 13. Each Ni(II) center adopts a pseudo-octahedral coordination geometry, with four sites being occupied by two different bptz ligands. The other two coordina-

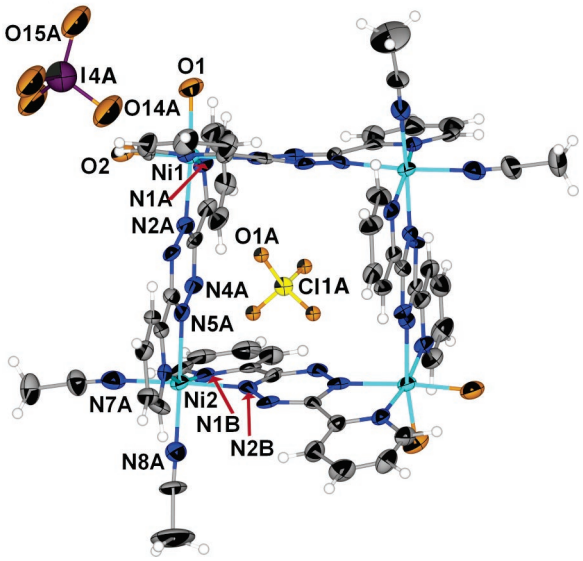

Figure 12. Thermal ellipsoid plot at the 50% probability level of the cationic unit $\{[\{Ni_4(bptz)_4(CH_3CN)_4(H_2O)_4\}\subset ClO_4][IO_4]\}^{6+}$ in **9**·3CH_3CN. Selected bond distances (Å) and angles (°): Ni1−O1 2.03(1), Ni1−N1A 2.07(1), Ni1−N2A 2.07(1), Ni2−N1B 2.05(2), Ni2−N7A 2.08(2), Ni2−N2B 2.06(1), Ni2−N5A 2.103(13), O2−Ni1−O1 86.6(5), O1−Ni1−N1A 92.9(5), O2−Ni1−N2A 87.4(5), O1−Ni1−N2A 169.4(6), N1B−Ni2−N7A 95.8(6), N1B−Ni2−N2B 78.6(6), N7A−Ni2−N2B 173.7(6), N1B−Ni2−N6A 163.6(6).

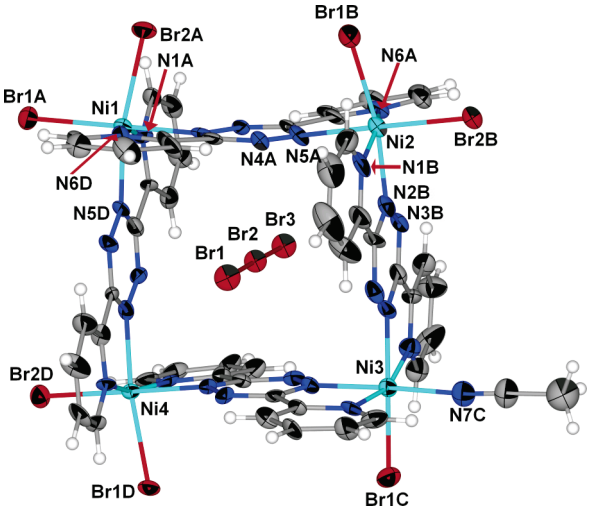

Figure 13. Thermal ellipsoid plot at the 50% probability level of $[\{Ni_4(bptz)_4(CH_3CN)Br_7\}\subset Br_3]$ in **10**·2CH_3CN·2.5C_7H_8. Selected bond distances (Å) and angles (°): Ni1−N1A 2.097(10), Ni1−N6D 2.079(10), Ni1−N5D 2.128(9), Ni1−Br1A 2.479(2), Ni1−Br2A 2.537(2), N1B−Ni2−N6A 161.1(4), N1A−Ni1−N2A 78.0(4), N6D−Ni1−N2A 89.1(4), N2A−Ni1−N5D 87.7(3), N1A−Ni1−Br1A 96.8(3), N2A−Ni1−Br1A 174.8(3), N1A−Ni1−Br2A 94.9(3), N6D−Ni1−Br2A 95.4(3), N2A−Ni1−Br2A 82.5(2), N5D−Ni1−Br2A 168.1(3), Br1A−Ni1−Br2A 97.59(7) Br1−Br2 2.525(2), Br2−Br3 2.566(2), Br1−Br2−Br3 179.17(7).

tion sites of the three Ni(II) ions are occupied by bromide ions, whereas a bromide ion and an acetonitrile molecule are coordinated to the fourth Ni(II) center. Presumably, replacement of the last acetonitrile molecule by bromide is not favored due to the fact that the Ni(II) square with the encapsulated $[Br_3]^-$ is neutral. The Ni···Ni distances are in the range of 6.806−6.915 Å, whereas the separations of the parallel tetrazine ring centroids are 6.638 and 7.014 Å. The Ni−N(bptz) distances are in the range 2.07(1)−2.128(9) Å, and the Ni3−N7C(CH_3CN) distance is 2.04(1) Å. The bptz ligands are nearly planar,

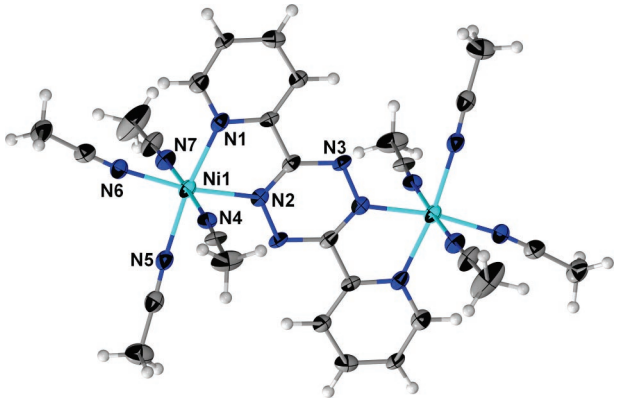

Figure 14. Thermal ellipsoid plot at the 50% probability level of the cationic unit $[Ni_2(bptz)(CH_3CN)_8]^{4+}$ in **11**. Selected bond distances (Å) and angles (°): Ni1−N1 2.067(7), Ni1−N4 2.072(6), Ni1−N7 2.045(7), N7−Ni1−N4 177.8(3), N4−Ni1−N5 86.1(2), N6−Ni1−N5 94.8(2), N1−Ni1−N4 89.8(2), N1−Ni1−N6 92.4(2), N7−Ni1−N2 90.9(2), N1−Ni1−N2 77.8(2).

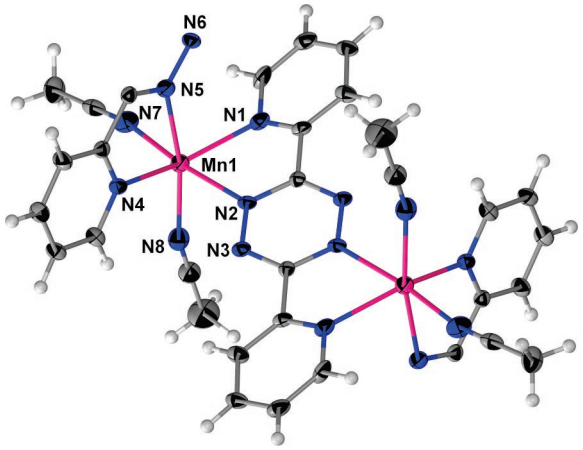

Figure 15. Thermal ellipsoid plot of the cationic repeat unit $[Mn_2(bptz)_2(CH_3CN)_4]^{4+}$ at the 50% probability level in the polymer **12**·1.5CH_3CN. Selected bond distances (Å) and angles (°): Mn1−N1 2.231(4), Mn1−N2 2.318(4), Mn1−N8 2.143(4), N7−Mn1−N5 172.4(2), N4−Mn1−N5 71.2(1), N5−Mn1−N2 94.5(1), N7−Mn1−N1 99.2(1).

and the $[Br_3]^-$ ion inside the cavity is parallel to the adjacent pairs of bptz ligands. The distances within the $[Br_3]^-$ anion are Br1−Br2 2.525(2) Å and Br2−Br3 2.566(2) Å.

$[Ni_2(bptz)(CH_3CN)_8][ClO_4]_4$ (11). Compound **11** consists of a dinuclear cation in which two Ni(II) ions are bridged by a bptz ligand. A thermal ellipsoid plot of the cationic unit $[Ni_2(bptz)(CH_3CN)_8]^{4+}$ is shown in Figure 14. Each metal ion is found in a distorted octahedral environment, with two sites being occupied by bptz and the remaining four sites capped by CH_3CN ligands. The midpoint of the tetrazine ring of the bptz ligand lies on an inversion center. The Ni1−N1(bptz−pyridyl) and Ni1−N2(bptz−tetrazine) distances are 2.067(7) and 2.078(7) Å, respectively, whereas the Ni1−N(CH_3CN) distances are in the range 2.045(7)−2.075(7) Å. The Ni···Ni distance is 6.904 Å, which is typical for the bptz-bridged Ni···Ni complexes.

$\{[Mn(bptz)(CH_3CN)_2][BF_4]_2\cdot 1.5CH_3CN\}_\infty$ (12·1.5CH_3CN). The structure of **12** consists of a cationic polymer in which two Mn(II) centers are bridged by bptz ligands that lie on inversion centers. A thermal ellipsoid plot of the $[Mn_2(bptz)_2(CH_3CN)_4]^{4+}$ unit is shown in Figure 15. The *trans* arrangement of the Mn−bptz units leads to formation of a polymeric structure rather than a discrete cyclic oligomer. Each Mn(II) center is in

a slightly distorted octahedral geometry, with two bptz units and two acetonitrile ligands completing the coordination sites. The Mn−N distances follow the same trend as other metallacyclophanes; namely, the shorter bonds are to the acetonitrile ligands (2.143(4) and 2.166(4) Å). The Mn−N(pyridyl) bond distances are 2.225(4) and 2.231(4) Å, and the Mn−N(tetrazine) distances are 2.318(4) and 2.313(4) Å. The Mn···Mn separation is 7.327 Å.

Discussion

Product Nuclearity Dependence on the Anion Identity. Considering the divergent nature of bptz and the absence of protective ligands around the Ni(II) and Zn(II) metal ions, the isolation of the discrete molecular squares **1**−**4** in high yields is quite remarkable. The formation of molecular squares is dominant in the presence of both $[BF_4]^-$ and $[ClO_4]$ ions, regardless of the presence of $[SbF_6]^-$ ions (Schemes 3 and 4). Other metallacages with encapsulated anions[36] have been reported to form in essentially quantitative yields as judged by NMR spectroscopy, but in many cases a variety of oligomeric species are detected.[37] The sufficient labilities of the Ni(II) and Zn(II) ions facilitate the conversion of intermediates into a single product by a *self-reorganization* mechanism, which reduces the likelihood of obtaining insoluble kinetic products and leads to formation of the square in high yields. This is supported by the fact that excess $[Zn(CH_3CN)_4][BF_4]_2$ leads to formation of the square $[Zn_4(bptz)_4(CH_3CN)_8][BF_4]_8$, as evidenced by ^{1}H NMR spectroscopy. The mass spectrometric data clearly point to the existence of intrinsically stable $[Ni_4]^{8+}$ (Figure 2) and $[Zn_4]^{8+}$ species (Figure S1) in the gas phase, in the presence of $[BF_4]^-$ and $[ClO_4]^-$ anions, with no evidence of higher nuclearity species such as the pentagon. Since both $[BF_4]^-$ and $[ClO_4]^-$ anions promote the formation of molecular squares with Ni(II) and Zn(II) ions (Scheme 1), presumably due to similarities in their size and shape,[25] it is reasonable to expect that molecular polygons of different nuclearities can form in the presence of other appropriate anions. The single crystal X-ray structural determination of $[\{Ni_5(bptz)_5(CH_3CN)_{10}\}\subset SbF_6]^{9+}$ revealed that the shape and size of the $[SbF_6]^-$ anion render it appropriate to occupy a cavity slightly larger than that of the square, viz., that of a pentagon (Figure 9).[13b] Furthermore, the ESI-MS studies of **5** in CH_3CN established that the $[Ni_5]^{10+}$ moiety persists in solution for long periods of time with no evidence of a $[Ni_4]^{8+}$ species (Figure 3). Therefore, the anion $[SbF_6]^-$ leads to the exclusive formation of the molecular pentagon both in the solid state and in solution.

The dictating role of the anion in these reactions is further corroborated by the formation of **6** from **5** in the presence of an excess amount of $[NO_3]^-$ anions. The existence of a possible molecular triangular unit is supported by the observation of a species at *m*/*z* 1194.7, which corresponds to $[Ni_3(bptz)_3(NO_3)_5]^+$ (Figure 4). Since X-ray-quality single crystals of **6** could not be obtained, despite numerous attempts, the identity of the triangle is supported solely by mass spectral data. It is important to note that the characteristic patterns for the $[Ni_5]^{10+}$ and $[Ni_4]^{8+}$ polygons are not evident in this spectrum, which suggests that the $[NO_3]^-$ anion is too small to template these higher nuclearity species.

Anion Selectivity of the Cavity. To further probe the anion selectivity in the molecular polygon formation, a solution of the pentagon **5** was treated with an equimolar mixture of $[BF_4]^-$ and $[PF_6]^-$ ions (Scheme 7). The single crystal X-ray structural determination of the resulting compound **8** showed it to be a molecular square in which a $[BF_4]^-$ ion resides inside the cavity (Figure 11), with one $[PF_6]^-$ and six $[SbF_6]^-$ outer-sphere anions. The $[PF_6]^-$ anion is not incorporated inside the cavity of the square, nor does its presence lead to a product of different nuclearity, facts which further underscore the importance of the anion size and shape in promoting a particular cyclic structure. Moreover, treatment of **2** with an excess of $[IO_4]^-$ leads to replacement of all the $[ClO_4]^-$ anions, except for the one residing inside the cavity (Scheme 8, Figure 12). Conversely, similar treatment of **2** with an excess of $[Br_3]^-$ ions leads to displacement of the $[ClO_4]^-$ with $[Br_3]^-$ ions (Scheme 9, Figure 13). Obviously, the larger tetrahedral anion $[IO_4]^-$ cannot replace $[ClO_4]^-$ inside the cavity, but the linear $[Br_3]^-$ anion is capable of doing so.

Apart from "weakly coordinating" anions, halides were also probed as possible templates in the chemistry of M(II) with bptz. Although reactions of halide salts with the pentagon **5** led to insoluble solids, in the case of [*n*-Bu_4N][I], a crop of crystals of the molecular square $[\{Ni_4(bptz)_4(CH_3CN)_8\}\subset I]^{7+}$ (**7**) with an encapsulated iodide ion was collected (Scheme 5, Figure 10). The fact that the spherical $[I]^-$ anion can template the formation of the square seems contradictory to the requirement of a specific anion geometry (namely tetrahedral) for the square to be formed, unless the size and polarizability of $[I]^-$ are taken into consideration; the large polarizability of iodide (19.22 $cm^3\ mol^{-1}$ in H_2O) allows it to adopt the directionality of a tetrahedral geometry.[38]

Stability of the Molecular Pentagon vs the Square. The competing influence of the anions in stabilizing the different cyclic entities was established by mass spectrometry and X-ray crystallography. The $[Ni_5]^{10+}$ pentagon **5** was found to be less stable compared to its $[Ni_4]^{8+}$ analogues **1** and **2**. Ion signals corresponding to the molecular square begin to appear in the ESI-MS spectra after addition of [*n*-Bu_4N][BF_4] or [*n*-Bu_4N]-[ClO_4] to a solution of **5**, and complete conversion of the Ni-(II) pentagon to the square is achieved by adding an excess of either tetrahedral anion (Scheme 3). Moreover, crystals of **1** are obtained from an acetonitrile solution of **5** that is layered over a saturated solution of [*n*-Bu_4N][BF_4] in benzene (Scheme 3). The aforementioned results underscore the ability of $[BF_4]^-$ and $[ClO_4]^-$ anions to template the formation of the molecular square even in the presence of $[SbF_6]^-$ ions (Scheme 4, Figure 16). The reverse conversion, namely that of the square to the pentagon, is also possible, albeit under more forcing conditions, viz., heating and longer reaction times (Scheme 3, Figures 5 and 16). Given the strain that is evident by the bowing of the bptz ligands in the pentagon (Figure 9),[13b] it is not unreasonable to expect that the square is intrinsically more stable than the pentagon. It is notable, however, that abstraction of the iodide

(36) Su, C.-Y.; Cai, Y.-P.; Chen, C.-L.; Lissner, F.; Kang, B.-S.; Kaim, W. *Angew. Chem., Int. Ed.* **2002**, *41*, 3371.
(37) (a) Takeda, N.; Umemoto, K.; Yamaguchi, K.; Fujita, M. *Nature* **1999**, *398*, 794. (b) Fujita, M.; Nagao, S.; Ogura, K. *J. Am. Chem. Soc.* **1995**, *117*, 1649. (c) Xu, J.; Parac, T. N.; Raymond, K. N. *Angew. Chem., Int. Ed.* **1999**, *38*, 2878.
(38) Bianchi, A.; García-España, E. Thermodynamics of Anion Complexation. In *Supramolecular Chemistry of Anions*; Bianchi, A., Bowman-James, K., García-España, E., Eds.; Wiley-VCH: New York, 1997; p 217.

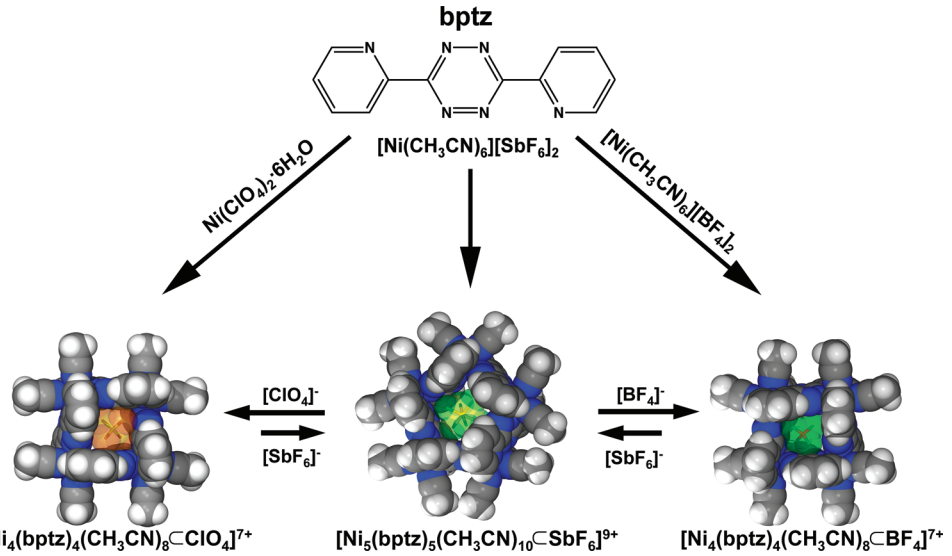

Figure 16. Space-filling representations of the cationic units $[\{Ni_5(bptz)_5(CH_3CN)_{10}\}\subset SbF_6]^{9+}$, $[\{Ni_4(bptz)_4(CH_3CN)_8\}\subset ClO_4]^{7+}$, and $[\{Ni_4(bptz)_4(CH_3CN)_8\}\subset BF_4]^{7+}$ and their scheme of interconversion.

from the cavity of the square **7** induces transformation of the latter to the less stable pentagon in the presence of $[SbF_6]^-$ ions (Scheme 6), a fact which suggests that a square lacking the appropriate encapsulated ion is not stable. Remarkably, the square and the pentagon are not interconverting in solution to form equilibrium mixtures in the absence of competing anions, as indicated by the ESI-MS spectra (Figures 2 and 3).

The high stability of the square is further supported by the fact that it is possible to exchange $[ClO_4]^-$ for $[Br_3]^-$ in the cavity of **2** (Scheme 9). Single crystal X-ray studies of $[\{Ni_4Br_7(bptz)_4(CH_3CN)\}\subset Br_3]$ reveal that the anion trapped inside the cavity is $[Br_3]^-$ and the parent cationic square remains intact, despite the fact that seven of the eight CH_3CN ligands have been replaced by bromide ions (Figure 13). This result is also promising in light of the potential to displace the acetonitrile ligands without degradation of the molecular square, a requisite condition for connecting individual square units via bridging ligands.

Divalent Transition Metals and Product Identity. The investigation of the reactions of other divalent transition metals, namely Mn(II), Fe(II), and Cu(II), with bptz supports the importance of the metal identity on the outcome of these reactions. Although the previous metals form the corresponding $[M_4(bptz)_4]^{8+}$ clusters, as evidenced by ESI-MS data recorded shortly after mixing the $M(ClO_4)_2{\cdot}xH_2O$ precursors with bptz in CH_3CN (Figures S2−S4), the $[M_4(bptz)_4]^{8+}$ species are not as stable as the corresponding Ni(II) and Zn(II) products (the signals for the tetranuclear adduct decrease over time with enhancement of the intensities of lower nuclearity species). The differences in stability may be due to subtle differences in the metal ions; for example, $[BF_4]^-$ or $[ClO_4]^-$ ions may not have the same tendency to template cyclic structures of various metals due to insufficient favorable contacts. In the case of the Cu(II) ion, the expected Jahn−Teller distortion could affect the formation of stable cyclic architectures such as molecular squares. It is thus apparent that the assembly of various metallacycles arises from an ideal match between the coordination preferences of the metal ions, the symmetry properties of the ligands,[39] and the anions present.

The reactions of solvated 3d metal ions with divergent ligands can, in principle, give rise to a variety of species. It is rare, however, to find examples in which open-chain oligomers or polymers are isolated from the same reaction that favors formation of molecular squares.[40] The reaction of $Ni(ClO_4)_2{\cdot}6H_2O$ with bptz affords, apart from the molecular square **2**, a small quantity of the dinuclear product $[Ni_2(bptz)(CH_3CN)_8][ClO_4]_4$ (**11**) (Figure 14), which suggests that the cyclic products **1** and **2** may be formed by dimerization of $[Ni_2]^{4+}$ intermediates. In the case of the bptz reactions with $[Mn(CH_3CN)_6][BF_4]_2$, a small quantity of the zigzag polymeric chain $\{[Mn(bptz)(CH_3CN)_2][BF_4]_2\}_\infty$ (**12**) (Figure 15) is formed. The isolation of **12** indicates that the formation of discrete cyclic products is not the only possible outcome, but is the result of the interplay between a variety of factors including anion, metal, and solvent identity.

It is important to note that, although both the Ni(II) and Zn(II) molecular squares are easily isolated in the solid state with the encapsulated anions $[BF_4]^-$ and $[ClO_4]^-$, their relative stabilities are quite different. In contrast to the Ni(II) squares, which are stable in solution for long periods of time, acetonitrile solutions of the $[Zn_4]^{8+}$ cations (in **3** and **4**) begin to decompose after approximately one week with deposition of insoluble precipitates, presumably polymeric in nature; this fact may be attributed to the greater lability of the Zn−N bonds. Moreover, unlike the Ni(II) analogue, the formation of $[Zn_4(bptz)_4(CH_3CN)_8]^{8+}$ is more sensitive to reaction conditions such as temperature and solvent (mass spectrometric studies indicate that the $[Zn_4]^{8+}$ species is formed only in CH_3CN).

Anion−π Interactions with the Cyclic Cations. Anions are known to occupy void spaces inside the cavities of macrocycles, a fact that is largely attributed to favorable crystal packing in the absence of any prominent noncovalent interactions.[41] In the space-filling representations of **1**, **2**, and **5** with the encapsulated

(39) Paul, R. L.; Bell, R. Z.; Jeffery, J. C.; McCleverty, J. A.; Ward, M. D. *Proc. Natl. Acad. Sci. U.S.A.* **2002**, *99*, 4883.
(40) (a) Tabellion, F. M.; Seidel, S. R.; Arif, A. M.; Stang, P. J. *J. Am. Chem. Soc.* **2001**, *123*, 11982. (b) Ellis, W. W.; Schmitz, M.; Arif, A. M.; Stang, P. J. *Inorg. Chem.* **2000**, *39*, 2547.

anions $[BF_4]^-$, $[ClO_4]^-$, and $[SbF_6]^-$, respectively, the efficiency of their packing in the metallacycles is nicely illustrated (Figure 16). Careful examination of the relevant structural parameters for **1**−**3**, **5**, and **7**−**9**, however, suggests that in the present cyclic structures there may be other stabilizing factors, such as anion−π interactions.[42] Short distances are noted between the centroids of the tetrazine rings to the O/F atoms of the encapsulated anions rather than interactions with the cationic metal centers.[39] Several theoretical studies of this type of anion−π interactions, recently undertaken by Frontera et al., suggest that they are energetically favorable.[42−46] A systematic investigation of N-heterocyclic ligands, with different degrees of electropositive character on the central π-ring systems, may reveal the degree to which such interactions dictate the formation and stabilization of a particular cyclic product. It is notable that several reports support the existence of such interactions on the basis of the anion location in the structure.[47]

Conclusions

The importance of the anions in the formation of cyclic molecules from a set of simple precursors has been demonstrated. The fact that the reaction between divalent metal ions and bptz can be tuned by the choice of counterion to favor a particular cyclic structure provides compelling evidence for an anion template effect in this chemistry. In particular, the tetrahedral anions $[BF_4]^-$ and $[ClO_4]^-$ act as templates in the formation of molecular squares with Ni(II) and Zn(II) ions and the bptz ligand. The anion $[SbF_6]^-$ was found to lead to the exclusive formation of a molecular pentagon with Ni(II), and mass spectrometric data suggest the existence of a molecular triangle in the presence of $[NO_3]^-$ anions. The molecular pentagon is less stable than the square, as evidenced by the facile conversion of $[\{Ni_5(bptz)_5(CH_3CN)_{10}\}\subset SbF_6]^{9+}$ to $[\{Ni_4(bptz)_4(CH_3CN)_8\}\subset BF_4]^{7+}$, $[\{Ni_4(bptz)_4(CH_3CN)_8\}\subset ClO_4]^{7+}$ (Figure 16), or $[\{Ni_4(bptz)_4(CH_3CN)_8\}\subset I]^{7+}$ by addition of excess quantities of $[BF_4]^-$, $[ClO_4]^-$, or $[I]^-$ anions to acetonitrile solutions of the pentagon, respectively (Schemes 3, 5, and 10). The conversion of the square to the pentagon requires heating and does not go to completion, as inferred from mass spectrometric data. Anion-exchange reactions of $[\{Ni_4(bptz)_4(CH_3CN)_8\}\subset ClO_4][ClO_4]_7$ indicate that, as expected, a larger anion such as $[IO_4]^-$ cannot replace $[ClO_4]^-$ inside the cavity, but that the linear $[Br_3]^-$ anion is capable of doing so. It can be concluded from this study that the nuclearity of the cyclic products is dictated by the identity of the anion present in solution during the self-assembly process. The latter may be attributed to a template effect that stabilizes one particular cyclic molecule over another due to favorable interactions between the anion inside the cavity and the bptz ligands. Given that there are close directional contacts between the anion and the central tetrazine ring of the bptz ligands, it is of interest to further explore the possibility of anion−π interactions being operative in dictating the outcome of these reactions.

Scheme 10

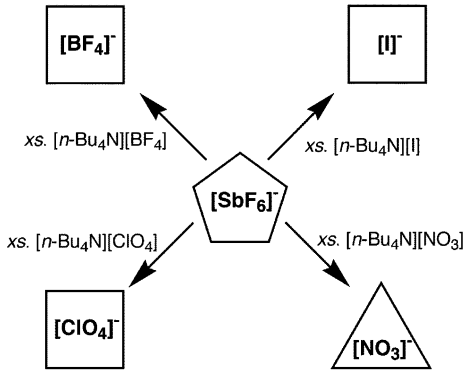

Acknowledgment. Prof. D. A. Singleton and Prof. F. P. Gabbai are acknowledged for helpful discussions. Dr. S. K. Silber and Dr. K. P. Sarathy (NMR facility of Chemistry Department) are acknowledged for their advice on the ^{19}F NMR spectra. We thank Dr. M. Shatruk and Dr. A. Chouai for assistance with the X-ray crystallography and the synthesis of bptz, respectively. K.R.D. gratefully acknowledges the Robert A. Welch Foundation and the National Science Foundation for a PI Grant (CHE-9906583), as well as for a grant to purchase the CCD X-ray equipment (CHE-9807975). D.H.R. gratefully acknowledges the National Institutes of Health (R01 RR019587) and the Robert A. Welch Foundation (A-1176). The NMR instrumentation was funded by NSF (CHE-0077917).

Supporting Information Available: Crystallographic data for **1**−**3**, **5**, **7**−**12** (CIF files). Figure S1, theoretical and experimental (ESI-MS) isotopic distribution patterns of the parent ion peak for $[Zn_4(bptz)_4(ClO_4)_7]^+$; Figure S2, ESI-MS spectrum of $[Mn_4(bptz)_4(CH_3CN)_8][ClO_4]_8$; Figure S3, ESI-MS spectrum of $[Fe_4(bptz)_4(CH_3CN)_8][ClO_4]_8$; Figure S4, ESI-MS spectrum of $[Cu_4(bptz)_4(CH_3CN)_8][ClO_4]_8$; Figure S5, ESI-MS spectra of the products from the reaction between $Ni(ClO_4)_2\cdot 6H_2O$ and bptz in acetonitrile, acetone, nitromethane, and ethanol; Figure S6, space-filling packing diagrams of $[\{Ni_4(bptz)_4(CH_3CN)_8\}\subset I][SbF_6]_7$ (**7**) and $[\{Ni_4(bptz)_4(CH_3CN)_8\}\subset ClO_4][ClO_4]_7$ (**2**). This material is available free of charge via the Internet at http://pubs.acs.org. CCDC depository numbers: **1**, CCDC-252137; **2**, CCDC-252537; **3**, CCDC-252906; **5**, CCDC-160210 and 275033; **7**, CCDC-253371; **8**, CCDC-254192; **9**, CCDC-253664; **10**, CCDC-254143; **11**, CCDC-254189; **12**, CCDC-254190.

JA052108Q

(41) Steed, J. W.; Juneja, R. K.; Atwood, J. L. *Angew. Chem., Int. Ed.* **1994**, *33*, 2456.
(42) (a) Garau, C.; Frontera, A.; Quinoñero, D.; Ballester, P.; Costa, A.; Deyà, P. M. *Recent Res. Dev. Chem. Phys.* **2004**, *5*, 227. (b) Garau, C.; Quinoñero, D.; Frontera, A.; Costa, A.; Ballester, P.; Deyà, P. M. *Chem. Phys. Lett.* **2003**, *370*, 7.
(43) (a) Quinoñero, D.; Garau, C.; Rotger, C.; Frontera, A.; Ballester, P.; Costa, A.; Deyà, P. M. *Angew. Chem., Int. Ed.* **2002**, *41*, 3389. (b) Quinoñero, D.; Garau, C.; Frontera, A.; Ballester, P.; Costa, A.; Deyà, P. M. *Chem. Phys. Lett.* **2002**, *359*, 486. (c) Garau, C.; Frontera, A. Quinoñero, D.; Ballester, P.; Costa, A.; Deyà, P. M. *ChemPhysChem* **2003**, *4*, 1344. (d) Garau, C.; Quinoñero, D.; Frontera, A.; Ballester, P.; Costa, A.; Deyà, P. M. *New J. Chem.* **2003**, *27*, 211. (e) Garau, C.; Frontera, A.; Quinoñero, D.; Ballester, P.; Costa, A.; Deyà, P. M. *Chem. Phys. Lett.* **2003**, *382*, 534. (f) Garau, C.; Frontera, A.; Quinoñero, D.; Ballester, P.; Costa, A.; Deyà, P. M. *Chem. Phys. Lett.* **2004**, *399*, 220. (g) Garau, C.; Frontera, A.; Quinoñero, D.; Ballester, P.; Costa, A.; Deyà, P. M. *J. Phys. Chem. A* **2004**, *108*, 9423. (h) Garau, C.; Frontera, A.; Quinoñero, D.; Ballester, P.; Costa, A.; Deyà, P. M. *Chem. Phys. Lett.* **2004**, *392*, 85.
(44) Mascal, M.; Armstrong, A.; Bartberger, M. D. *J. Am. Chem. Soc.* **2002**, *124*, 6274.
(45) Yaroslav, R. S.; Lindeman, S. V.; Rosokha, S. V.; Kochi, J. K. *Angew. Chem., Int. Ed.* **2004**, *43*, 4650.
(46) Kim, D.; Tarakeshwar, P.; Kwang, S. K. *J. Phys. Chem. A* **2004**, *108*, 1250.
(47) (a) Schottel, B. L.; Bacsa, J.; Dunbar, K. R. *Chem. Commun.* **2005**, 46. (b) de Hoog, P.; Gamez, P.; Mutikainen, I.; Turpeinen, U.; Reedijk, J. *Angew. Chem., Int. Ed.* **2004**, *43*, 5815. (c) Demeshko, S.; Dechert, S.; Meyer, F. *J. Am. Chem. Soc.* **2004**, *126*, 4508.